Clonal evolution of adult T-cell leukemia/lymphoma takes place in the lymph nodes

Akira Umino,[1,2] Masao Nakagawa,[1] Atae Utsunomiya,[3] Kunihiro Tsukasaki,[4] Naoya Taira,[5] Naoyuki Katayama,[2] and Masao Seto[1,6]

[1]Division of Molecular Medicine, Aichi Cancer Center Research Institute, Nagoya, Japan; [2]Hematology and Oncology, Mie University Graduate School of Medicine, Tsu, Japan; [3]Department of Hematology, Imamura Bun-in Hospital, Kamoikeshinmachi, Kagoshima, Japan; [4]Department of Hematology and Molecular Medicine Unit, Atomic Bomb Disease Institute, Nagasaki University Graduate School of Biomedical Sciences, Nagasaki, Japan; [5]Deptment of Internal Medicine, Heartlife Hospital, Okinawa, Japan; and [6]Department of Cancer Genetics, Nagoya University Graduate School of Medicine, Chikusa-ku, Nagoya, Japan

Adult T-cell leukemia/lymphoma (ATLL) is the neoplasm caused by human T-cell leukemia virus type 1 (HTLV-1). We performed oligo-array comparative genomic hybridization (CGH) against paired samples comprising peripheral blood (PB) and lymph node (LN) samples from 13 patients with acute ATLL. We found that the genome profiles of the PB frequently differed from those of the LN samples. The results showed that 9 of 13 cases investigated had a log2 ratio imbalance among chromosomes, and that chromosome imbalances were more frequent in LN samples. Detailed analysis revealed that the imbalances were likely caused by the presence of multiple subclones in the LN samples. Five of 13 cases showed homozygous loss regions in PB samples, which were not found in the LN samples, indicating that tumors in the PB were derived from LN subclones in most cases. Southern blot analysis of TCRγ showed that these multiple subclones originated from a common clone. We concluded that in many ATLL cases, multiple subclones in the LNs originate from a common clone, and that a selected subclone among the LN subclones appears in the PB. (*Blood*. 2011;117(20):5473-5478)

Introduction

Adult T-cell leukemia/lymphoma (ATLL) is the neoplasm caused by human T-cell leukemia virus type 1 (HTLV-1). The disease is associated with poor prognosis due to drug resistance, the occurrence of opportunistic infections, a large tumor burden with multi-organ failure, and hypercalcemia. Shimoyama et al[1] classified ATLL into 4 subtypes: smoldering, chronic, lymphoma, and acute. It is also known that HTLV-1 infection alone does not facilitate the progress of infected $CD4^+$ T cells to fully malignant ATLL cells. Therefore, the search for genes involved in ATLL development and for the specific genes involved in each ATLL type has been actively pursued, albeit with limited success. ATLL-specific chromosomal abnormalities have yet to be found; however, a frequent abnormality found in ATLL is 14q11, which has also been found in other types of T-cell malignancies.[2,3] HTLV-1 provirus integration sites have also been extensively sought, and the sites identified were found to be randomly located. Investigations relying on G-band and fluorescence in situ hybridization analyses have not been fruitful in providing a detailed delineation of the genomic aberrations involved.[4] The use of high-resolution, array-based comparative genomic hybridization (CGH) for comprehensive chromosome analysis should prove useful in the search for genomic aberrations. We showed previously that acute and lymphoma ATLL types possess distinct genomic profiles, as determined by bacterial artificial chromosome array CGH.[5] It should be noted, however, that when lymphoma-type ATLL progresses to manifest more than 2% flower cells in the peripheral blood (PB), it is then classified as the acute type. We set out to analyze the genomic aberrations of acute-type ATLL with paired PB and lymph node (LN) samples in more detail by oligo-array CGH.

An important factor in the diagnosis of ATLL is the identification of monoclonal integration of HTLV-1. It has been reported that the same HTLV-1–infected clone was detected over several years in a chronic-type ATLL patient.[6,7] These types of HTLV-1–infected $CD4^+$ T lymphocytes are believed to accumulate various changes during an extensive latency period of over 50 years.[8] Alterations in genomic copy number represent one example of the type of accumulated genomic changes that can occur. In the present study, we performed high-resolution oligo-array CGH (Agilent Technologies) using a 44 000-probe set against paired samples obtained from the PB and LNs of 13 patients with acute-type ATLL.

Methods

ATLL patients and cell lines

We conducted a survey of genomic profiles by examination of PB and LN samples taken from 13 patients with acute-type ATLL. Paired samples were collected from each patient within 14 days of diagnosis. The PB and LN samples, together with clinical data, were obtained from 13 patients under a protocol approved by the institutional review board of the Aichi Cancer Center. Informed consent was provided according to the Declaration of Helsinki. Patients were diagnosed from those hospitalized between 1988 and 2010 at Imamura-Bunin Hospital and Nagasaki University School of Medicine. The diagnosis of ATLL was based on clinical features, hematologic characteristics, immunophenotype, and the presence of serum antibodies to ATLL-associated antigens. The median age of the patients was

Submitted December 26, 2010; accepted March 11, 2011. Prepublished online as *Blood* First Edition paper, March 29, 2011; DOI 10.1182/blood-2010-12-327791.

The online version of this article contains a data supplement.

The publication costs of this article were defrayed in part by page charge payment. Therefore, and solely to indicate this fact, this article is hereby marked "advertisement" in accordance with 18 USC section 1734.

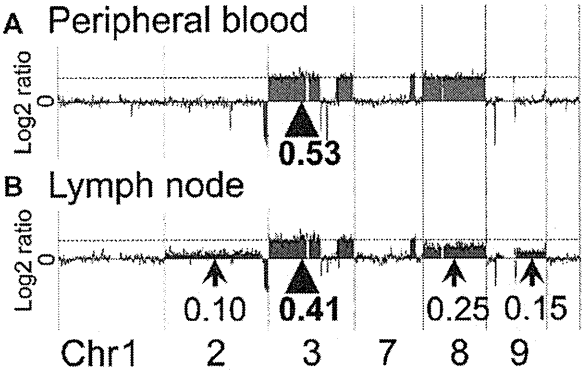

Figure 1. Representative profiles of the PB and LN samples of case 1. Array CGH results for case 1 are shown. (A) In the PB sample of case 1, regions of gain were detected. The log2 ratio of chromosome 3 was 0.53 (arrowhead). The log2 ratios of chromosomes 7 and 8 were the same as for chromosome 3 (dotted line). (B) In the LN sample of case 1, a log2 ratio imbalance was found. Log2 ratios among chromosomes 2, 3, 7, 8, and 9 differed. The log2 ratios of chromosome 3 and 7 were 0.41 (arrowhead and dotted line). Arrows show different log2 ratios: chromosome 2 = 0.10, chromosome 8 = 0.25, and chromosome 9 = 0.15.

57 years (range, 32-74 years). Detailed patient information is provided in supplemental Table 1 (available on the *Blood* Web site; see the Supplemental Materials link at the top of the online article).

Four cell lines, SP-49,[9] HANK1,[10] ATN-1,[11] and Jurkat,[12] were also analyzed. SP-49 is a mantle cell lymphoma cell line, HANK1 is a natural killer/T-cell lymphoma line, ATN-1 is an ATLL cell line, and Jurkat is a T-cell lymphoblast–like cell line.

Peripheral blood samples were obtained from the blood of 8 healthy male donors. PBMCs were isolated by Ficoll-Paque PLUS centrifugation (GE Healthcare).

DNA extraction

$CD4^+$ cells in PB samples were purified using a magnetic-activated cell-sorting protocol (Miltenyi Biotec). High–molecular-weight DNA was extracted from $CD4^+$ cells, frozen LNs, and from the SP-49, HANK1, ATN-1, and Jurkat cell lines using standard proteinase K treatment and phenol-chloroform extraction.[13] Normal DNA was obtained from PBMC samples of 8 healthy male donors.

Oligo-array CGH

Characterization of the genomic aberrations was performed using Agilent 44K Whole Human Genome CGH arrays (Agilent Technologies) containing 44 000 probes. Procedures for DNA digestion, labeling, hybridization, scanning, and data analyses were performed according to the manufacturer's protocol (Agilent Technologies).

CGH data analysis

CGH data were extracted from scanned images using Feature Extraction software (version 10.3; Agilent Technologies). Raw data were transferred to the Genomic Workbench v5.0 software (Agilent Technologies) for further analysis. We defined gains and losses over a continuous 15-probe dataset as a linear log2 ratio average of ≥ 0.05 or ≤ -0.05, respectively, and microdeletion for a range of 3-15 probes as a linear log2 ratio average of ≤ -0.4. A detailed explanation of the log2 ratio is available in the supplemental data. The array CGH data have been deposited in ArrayExpress under the accession number E-MEXP-3042.

Southern blot analysis of HTLV-1 integration and TCRγ rearrangement

Integration of the HTLV-1 provirus genome and TCRγ rearrangement were assayed as described previously.[5,14] In brief, DNA samples (5 μg) of LNs were digested with restriction enzymes (PstI) and electrophoresed through 0.7% agarose gels. The DNA was then transferred onto a Hybond N^+ membrane (Amersham Pharmacia Biotech) and hybridized to randomly primed ^{32}P-labeled DNA probes specific for the HTLV-1 and TCRγ genes. Blots were then washed at the appropriate stringency and visualized by autoradiography. The HTLV-1 probe comprised a 1.0-kb fragment of the pX region, which was PCR amplified using the primers 5′-ccacttcccagggtttggacag-3′ and 5′-tctgcctctttttcgttaaaaagtagagaaatggg-3′, and the TCRγ probe comprised a 0.6-kb fragment of Jγ2.1.[14]

Results

Oligo-array CGH analysis against paired samples obtained from the PB and LNs

In all of the 13 acute-type ATLL cases, genomic aberrations were detected by oligo-array CGH. Representative profiles of the paired samples obtained from the PB and LNs in cases 1 and 2 are shown in Figure 1A and B and Figure 2A and B, respectively.

In the PB sample of case 1, genomic aberration regions showed a constant log2 ratio. Regions of gain were detected on chromosomes 3, 7, and 8. The log2 ratios corresponding to these regions were 0.53, suggesting that there was no imbalance (Figure 1A arrowhead). On the other hand, imbalance of the log2 ratio among chromosomes was found for the LN sample of case 1. Genomic aberrations of the case 1 LN sample were similar to

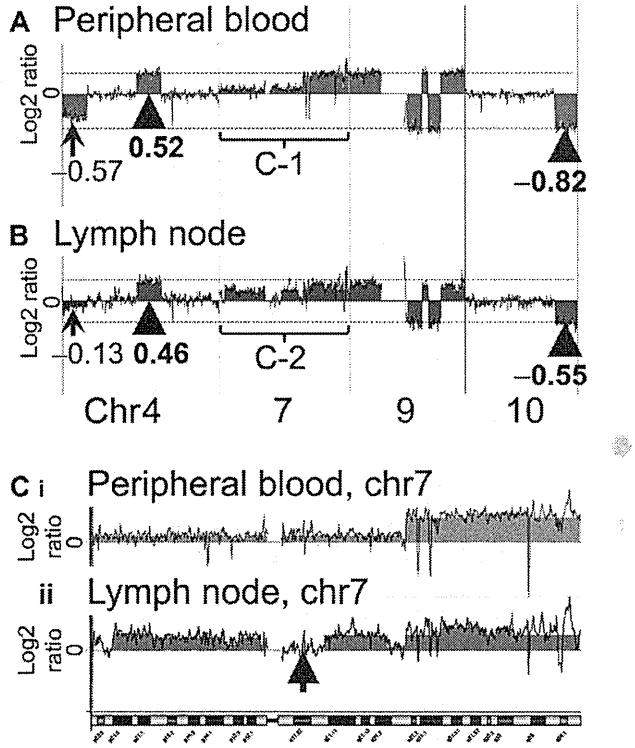

Figure 2. Representative profiles of the PB and LN samples of case 2. The results for case 2 were more complex than those for case 1. In both the PB and the LN samples of case 2, a log2 ratio imbalance was found. (A) In the PB sample, the arrowhead and dotted line indicate the majority of log2 ratios of gain and loss regions. Log2 ratios of the majority of loss regions were −0.82. The log2 ratio of chromosome 4 was −0.57. (B) In the LN sample, the arrowhead and dotted line indicate the majority of log2 ratios of gain and loss regions. Log2 ratios of the majority of loss regions were −0.55. The log2 ratio of chromosome 4 was −0.13. Chromosome 7 regions of PB and LN samples are magnified as Ci and Cii, respectively. (C) Chromosome 7 of the case 2 PB sample shows complex aberrations (i). This result also indicates a log2 ratio imbalance. Chromosome 7 of the case 2 LN sample shows more complex aberrations (ii). An arrow indicates a region (7q11.21-11q.23) without genomic aberration. Ci and Cii suggest that the genomic profiles of the PB and LN samples differ.

Table 1. Array CGH results of paired samples of acute-type ATLL

Case no.	Genome aberrations	Log2 imbalance		Genomic profiles of PB and LN	Common aberration regions between PB and LN	ATLL clones
		PB	LN			
1	+	−	+	different	+	Multiple subclones
2	+	+	+	different	+	Multiple subclones
3	+	−	−	same	+	Monoclone
4	+	+	+	different	+	Multiple subclones
5	+	+	−	different	+	Multiple subclones
6	+	−	−	same	+	Monoclone
7	+	+	+	different	+	Multiple subclones
8	+	−	+	different	+	Multiple subclones
9	+	−	+	different	+	Multiple subclones
10	+	−	+	different	+	Multiple subclones
11	+	−	−	same	+	Monoclone
12	+	−	−	same	+	Monoclone
13	+	+	+	different	+	Multiple subclones
Total	13 (100%)	5 (38.4%)	8 (61.5%)	9 (69.2%)	13 (100%)	9 (69.2%)

+ indicates present; and −, absent.

that of the PB sample. However, the log2 ratios among chromosomes 2, 3, 7, 8, and 9 differed as follows. Regions of gain were detected on chromosomes 2, 3, 7, 8, and 9, as shown by the log2 ratios: chromosome 2 = 0.10, chromosomes 3 and 7 = 0.41, chromosome 8 = 0.25, and chromosome 9 = 0.15 (Figure 1B arrowhead and arrows). The log2 ratio of chromosome 8 was lower than that of chromosomes 3 and 7. Gains of chromosomes 2 and 9 were detected in the LN sample, but not in the PB sample. These results indicated that a log2 ratio imbalance occurred in the LN sample.

Case 2 had a log2 ratio imbalance in both the PB and LN samples (Figure 2A). The genomic aberrations of the case 2 PB sample differed from those of the LN sample, as was also found with case 1. In the case 2 PB sample, regions of loss were detected on chromosomes 4, 9, and 10, as shown by the log2 ratios: chromosome 4 = −0.57 (Figure 2A arrow) and chromosomes 9 and 10 = −0.82 (Figure 2A arrowhead and dotted line). In the case 2 LN sample, regions of loss were also detected on chromosomes 4, 9, and 10, as shown by the log2 ratios: chromosome 4 = −0.13 (Figure 2B arrow) and, chromosomes 9 and 10 = −0.55 (Figure 2B arrowhead and dotted line). These data indicated that both samples had a log2 ratio imbalance. Complex genome aberrations were found for chromosome 7 in the paired samples of case 2. Consecutive gain regions were found in the whole of chromosome 7 of the PB sample (Figure 2Ci, and a region (7q11.21-11q.23) without genomic aberrations was found in chromosome 7 of the LN sample (Figure 2Cii arrow).

A log2 ratio imbalance among chromosomes was present in many other samples of acute-type ATLL, as summarized in Table 1.

Confirmation of log2 ratio imbalance among chromosomes

A log2 ratio imbalance among chromosomes was found in many ATLL clinical samples. We expected that a log2 ratio imbalance would indicate the presence of clones with different genomic aberrations. Therefore, we prepared 2 cell lines, SP-49 and HANK1, which possess different genomic aberrations. The genomic DNA of SP-49 was mixed with that of HANK1. We then conducted oligo-array CGH using the mixed-genomic DNA samples at various ratios.

Array CGH analysis of the SP-49 genome showed some genomic aberration regions, which were consistent with the G-band result that had been reported.[9] Log2 ratios of all 1-copy gain regions were 0.55, and log2 ratios of all 1-copy loss regions were −0.80. Imbalance of the log2 ratio among the chromosomes was not found. The same was true for HANK1, in which genomic aberration regions were consistent with the G-band result that had been reported and an imbalance of the log2 ratio among the chromosomes was not found.[10]

A representative array CGH result using a mixed-DNA sample at a ratio of 7:3 (SP-49:HANK1) is shown in Figure 3. The results showed an imbalance of the log2 ratio among chromosomes. It was possible to reproduce the log2 ratio imbalance. For example, the log2 ratios of chromosomes 2p14-pter, 2q14.3-qter, and 7p were 0.55, 0.15, and 0.46, respectively. These log2 ratios clearly differed. Furthermore, additional regions with different log2 ratios were found.

These results indicated that some of the clones present in the sample that had different genome profiles caused a log2 ratio imbalance in the array CGH result. The log2 ratio did not differ in chromosome 2p, which had a copy region identical to both SP-49 and HANK1.

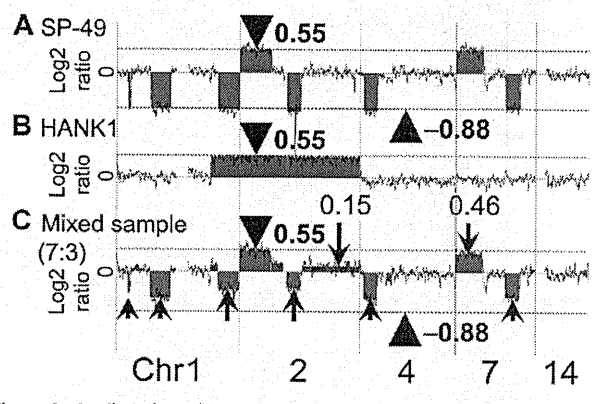

Figure 3. Confirmation of log2 ratio imbalance among chromosomes. The manner in which the log2 ratio imbalance occurred was confirmed. (A) SP-49 showed no imbalance. Log2 ratios of gain regions were 0.55 (arrowhead and dotted line). Log2 ratios of loss regions were −0.88 (arrowhead and dotted line). (B) HANK1 showed no imbalance. Log2 ratios of gain regions were 0.55 (arrowhead and dotted line). (C) Mixed-genomic DNA at a ratio of 7:3 reproduced the log2 ratio imbalance. The log2 ratio of chromosome 2p14-pter of the mixed DNA sample was 0.55 (arrowhead). Chromosome 2p had a copy region identical to both SP-49 and HANK1. Arrows indicate the log2 ratio imbalance.

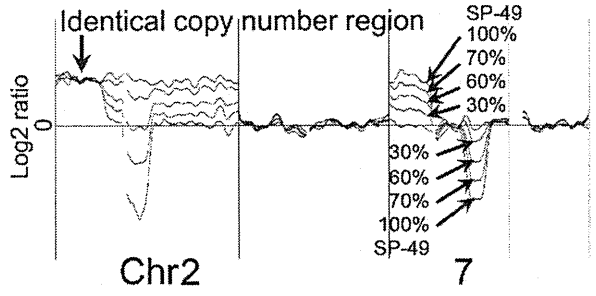

Figure 4. Log2 ratio reflects the ratio of tumor. The genome profiles of mixed-DNA samples comprising various ratios were superimposed. Gain was detected in chromosome 7 of all mixed samples, as shown by the log2 ratio: SP-49 = 0.55; 100%, 7:3 = 0.46; 70%, 6:4 = 0.32; 60%, 3:7 = 0.20; 30%. Loss was also detected in chromosome 7 of all mixed samples as shown by the log2 ratio: Sp-49 = −0.88; 100%, 7:3 = −0.62; 70%, 6:4 = −0.39; 60%, 3:7 = −0.14; 30%. Chromosome 2p had a copy region identical to both SP-49 and HANK1. The log2 ratios never changed in these regions.

Log2 ratios reflect the ratio of tumor

The genome profiles of mixed-DNA samples comprising various ratios were superimposed (Figure 4). The ratios of SP-49 to HANK1 were 7:3, 6:4, and 3:7. These results clearly revealed that the log2 ratio reflected the ratio of the tumor. When tumors included in a sample had identical genomic aberration regions, the log2 ratio never changed in these regions.

Southern blot analysis of HTLV-1 integration and TCRγ rearrangement

HTLV-1 integration

HTLV-1 integration was examined using Southern blot analysis, and the results showed HTLV-1 integration in all of the 11 cases examined. Eight of the 11 cases examined comprised a mono-integration band, whereas the others showed multi-integration bands. (Figure 5A)

TCRγ rearrangement

Southern blot analysis of TCR Jγ rearrangement was also conducted and evaluated as described previously by Moreau et al.[14] The results indicated that all samples were monoclonal (Figure 5B). Five of the 11 cases examined had a 6.8-kb rearrangement band, and 2 had a 2.9-kb rearrangement band. The others showed loss of germinal bands. In case 2, one allele of TCRγ was rearranged, because the germinal band of 8.0 kb was weaker than that of 4.9 kb. Case 7 lost all germinal bands, such as ATN-1, which is an ATLL cell line. This result indicated that both alleles of TCRγ were rearranged at Jγ2.3, because no deletion was found in case 7 by array CGH. Given that 3 or more TCR rearrangement bands were not found, no cases showed definite multi-clonality in tumor cells. These results indicated that the acute-type ATLL examined represented a monoclonal tumor comprising TCR rearrangements and with some possessing multiple integrations of HTLV-1.

Appearance of LN subclones before PB subclones

Array CGH analysis revealed that PB samples from 5 of 13 cases had homozygous loss regions that were not found in the corresponding LN samples of each case. In case 2, 1p12-1p13.1 of the PB sample was seen to represent homozygous loss, unlike the case with the LN sample (Figure 6). However, log2 ratios of same region in the LN sample seemed to be slightly lower than those of neighboring regions. This raised the possibility that a minor

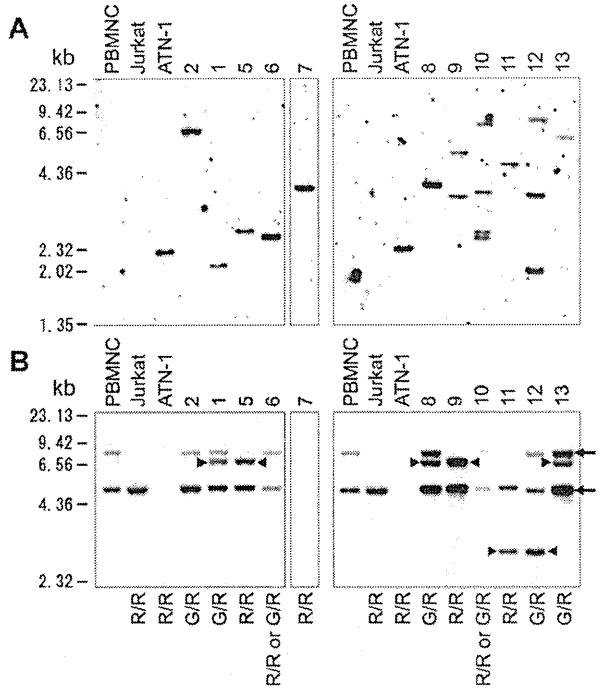

Figure 5. Southern blot analysis. (A) Southern blot analysis of HTLV-1 integration in 11 of 13 cases. (B) Southern blot analysis of TCRγ rearrangement. Arrows indicate the 8.00- and 4.9-kb germline bands. Arrowheads indicate the 6.8- and 2.9-kb rearrangement bands. G indicates a germinal allele; R, rearrangement allele; G/R, rearrangement of one allele; R/R, rearrangement of both alleles.

subclone was present. The PB samples from cases 1, 4, 8, and 10 also had homozygous loss regions that were not clearly found in the corresponding LN samples (Table 2).

No cases had a homozygous loss region in the LN samples when the PB samples had a heterozygous loss in the same regions. Array CGH and Southern blotting results indicated that multiple subclones had developed from one clone. Therefore, when 2 clones were found in a patient, the clone with homozygous loss must have developed from the clone with heterozygous loss. The homozygous loss analysis revealed that in about 40% of ATLL patients, subclones that had appeared in the PB were derived from LN subclones.

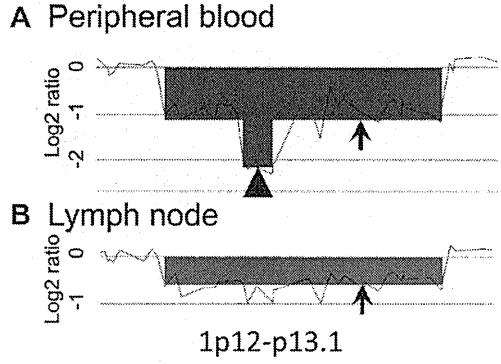

Figure 6. Homozygous loss region analysis. A representative homozygous loss region of case 2 is shown (1p12-p13.1). The total scale of the figure is approximately 2 Mb. The arrowhead indicates a homozygous loss region; arrows indicate heterozygous loss regions. Homozygous loss was found only in the PB sample. The log2 ratio of this region in the LN sample was slightly lower than that in the neighboring regions, suggesting the possibility that a minor subclone may exist in the LNs.

Table 2. PB samples of 5 of 13 cases only had homozygous loss regions that were not found in the LN samples

Case no.	Homozygous loss only in PB	Homozygous loss only in LN	Locus	Gene
1	+	–	3q22.3	*PCCB, STAG1*
2	+	–	1p12-p13.1	*IGSF3*
3	–	–		
4	+	–	6p22.3	*ATXN1*
5	–	–		
6	–	–		
7	–	–		
8	+	–	4q31.21	*INPP4B*
9	–	–		
10	+	–	9q31.2	*KLF4*
11	–	–		
12	–	–		
13	–	–		
Total	5	0		

+ indicates present; and –, absent.

Selected subclone of LNs in the PB

Tumor cells in the PB samples of some cases (eg, cases 1 and 9) appeared to have been selected from multiple subclones. In these cases, a log2 ratio imbalance was not found in the PB sample but was found in the LN sample. This indicated that PB samples were monoclonal and that the LN samples contained multiple subclones. Both samples from each case had common aberrations, and the LN samples had aberrations that were not found in the PB samples. These results may indicate that the LNs contain multiple subclones with different genomic aberrations, and that one of these subclones then appears in the PB (Figure 7).

Discussion

The imbalance and differing genomic profiles of PB and LN samples indicate that acute-type ATLL comprises multiple subclones

In this study, we revealed the presence of a log2 ratio imbalance among chromosomes of LN samples in many patients with acute-type ATLL. Most of the genomic profiles were found to differ from those of the PB samples. Although monoclonal proliferation of acute-type ATLL is referred to in the World Health Organization classification,[15] these data clearly show that acute-type ATLL contains multiple subclones that originate as a result of clonal evolution in ATLL patients.

Shinawi et al[16] reported a case of pediatric AML in which 2 clones with different chromosome aberrations showed a log2 ratio imbalance as detected by array CGH. We were able to reproduce a log2 ratio imbalance among chromosomes by mixing different ratios of DNA prepared from 2 different cell lines. The log2 ratio reflected the ratio of tumor clones. Based on these data, we analyzed the acute-type ATLL data and identified that a log2 ratio imbalance indicated the presence of multiple subclones in a sample. Minority clones with low log2 ratios could be found in this experiment by taking advantage of the high sensitivity associated with the use of array CGH. As a result, the presence of multiple subclones was unambiguously determined.

Cases showing different genomic profiles between PB and LN samples reached as high as 69%. We reported previously that paired samples obtained from different sites had different chromosomal aberrations in some cases.[17] We also reported that sequential samples at chronic and crisis or acute onset and relapse in each case showed different chromosome aberrations or integrations as determined by chromosomal CGH or Southern blot analysis.[17] Similar clonal change has been reported previously in some cases of B-cell lymphoma.[18] Although analysis of sequential samples is important when examining the stability of multiple subclones, it is difficult to acquire sequential samples from acute-type ATLL patients because these patients require immediate chemotherapy. However, chronic-type ATLL can be treated with "watchful waiting," so the clonal stability of ATLL may be explored in these patients.

Our data indicate that acute-type ATLL comprises multiple subclones with differing genomic aberrations. Several morphologic variants of ATLL have been described,[15] and the presence of a mixture of cells of different sizes has been reported. However, the histological type does not correspond to the clinical subtype.[19] Therefore, it is reasonable to postulate that the histological type does not always reflect the clinical features because the tumor subclones may differ at various sites.

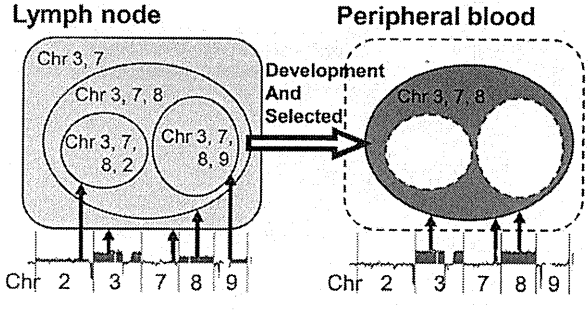

Figure 7. Selected subclone from the LN in the PB. Shown is a schematic representation of a selected subclone from the LN sample in the PB of case 1. In the LN sample of case 1, at least 4 subclones exist: a subclone with chromosome 3 and 7 aberrations; a subclone with additional chromosome 8 aberrations; a subclone with chromosome 3, 7, 8, and 2 aberrations; and a subclone with chromosome 3, 7, 8, and 9 aberrations. Among these subclones, a subclone with chromosome 3, 7, and 8 aberrations appeared in the PB sample.

HTLV-1 integration and TCRγ rearrangement determined by Southern blotting

We focused on the cell origin of the multiple subclones in each patient. Southern blot analysis revealed a monoclonal band of HTLV-1 integration or monoclonal rearrangement of TCRγ in all samples examined. These data indicated that the ATLL clones in each case had a common tumor cell origin. ATLL research and treatment utilize the Shimoyama classification. Acute-type ATLL represents one subtype in the classification, and is considered to be a monoclonal tumor. Our data are also consistent with this classification. However, it is possible that multiple subclones in the LNs possess a diversity that may account for the variable clinical manifestations and drug resistance that can occur during the treatment of ATLL.

Selection of leukemic clone and diversity in LNs

Array CGH suggested that the subclones in the PB and LNs differed even though they are derived from an identical monoclonal tumor cell, as determined by in Southern blot analysis. Given that the clones are derived from one clone, theoretically the clone with heterozygous loss is never derived from a cell with homozygous loss. Homozygous loss regions were only present in the PB samples examined at a frequency of 38% (5 of 13 cases examined). None of the 5 samples showed homozygous loss

regions found in the LN samples, indicating that in these cases, subclones present in the LNs were not derived from those in the PB. These results suggested that the selected subclones appeared in the PB after subclones developed in the LNs. However, it remains to be determined how these clones in the PB become stable during the course of disease. It is also important to determine whether the tumor cells in the PB can proliferate at the level of tumor cells in the LNs.

In conclusion, the results of the present study showed that there are multiple subclones in acute-type ATLL, all of which possess a common TCR rearrangement and the genomic profiles of which often differ between the PB and LNs. Cases were identified in which a selected subclone from multiple subclones in the LN samples was also identified in the PB samples. ATLL was clinically classified into 4 subtypes by Shimoyama. However, the specific genes that characterize acute-type ATLL have not been identified. Our results reveal that acute-type ATLL is a genetically heterogeneous neoplasm and that clonal evolution of ATLL takes place in the LNs.

Acknowledgments

We thank Dr Koichi Ohshima for diagnoses; Dr Shinobu Tsuzuki, Dr Kennosuke Karube, and Dr Keiichiro Honma for discussions and encouragement throughout this study; and Kyoko Hirano for outstanding technical assistance.

This work was supported in part by grants-in-aid from the Ministry of Health, Labor and Welfare of Japan; from the Ministry of Education, Culture, Sports, Science and Technology of Japan; and from the Japan Society for the Promotion of Science.

Authorship

Contribution: A. Umino performed the experiments, analyzed data, and wrote the paper; M.N. analyzed data and performed experiments; A. Utsunomiya provided advice, discussed clinical data, and treated patients; K.T. provided advice, discussed clinical data, treated patients, and wrote the paper; N.T. analyzed and discussed clinical data; N.K. discussed clinical data; and M.S. supervised the research, discussed clinical data, analyzed data, and wrote the paper.

Conflict-of-interest disclosure: The authors declare no competing financial interests.

Correspondence: Masao Seto, MD, PhD, Division of Molecular Medicine, Aichi Cancer Center Research Institute, 1-1 Kanokoden, Chikusa-ku, Nagoya, Aichi 464-8681, Japan; e-mail: mseto@aichi-cc.jp.

References

1. Shimoyama M. Diagnostic criteria and classification of clinical subtypes of adult T-cell leukaemia-lymphoma. A report from the Lymphoma Study Group (1984-87). *Br J Haematol.* 1991;79(3):428-437.
2. Raimondi SC, Behm FG, Roberson PK, et al. Cytogenetics of childhood T-cell leukemia. *Blood.* 1988;72(5):1560-1566.
3. Shimoyama M, Abe T, Miyamoto K, et al. Chromosome aberrations and clinical features of adult T cell leukemia-lymphoma not associated with human T cell leukemia virus type I. *Blood.* 1987; 69(4):984-989.
4. Maciejewski JP, Tiu RV, O'Keefe C. Application of array-based whole genome scanning technologies as a cytogenetic tool in haematological malignancies. *Br J Haematol.* 2009;146(5):479-488.
5. Oshiro A, Tagawa H, Ohshima K, et al. Identification of subtype-specific genomic alterations in aggressive adult T-cell leukemia/lymphoma. *Blood.* 2006;107(11):4500-4507.
6. Tsukasaki K, Tsushima H, Yamamura M, et al. Integration patterns of HTLV-I provirus in relation to the clinical course of ATL: frequent clonal change at crisis from indolent disease. *Blood.* 1997;89(3):948-956.
7. Etoh K, Tamiya S, Yamaguchi K, et al. Persistent clonal proliferation of human T-lymphotropic virus type I-infected cells in vivo. *Cancer Res.* 1997; 57(21):4862-4867.
8. Okamoto T, Ohno Y, Tsugane S, et al. Multi-step carcinogenesis model for adult T-cell leukemia. *Jpn J Cancer Res.* 1989;80(3):191-195.
9. Daibata M, Takasaki M, Hirose S, et al. Establishment of a new human B cell line carrying t(11;14) chromosome abnormality. *Jpn J Cancer Res.* 1987;78(11):1182-1185.
10. Kagami Y, Nakamura S, Suzuki R, et al. Establishment of an IL-2-dependent cell line derived from 'nasal-type' NK/T-cell lymphoma of CD2+, sCD3-, CD3epsilon+, CD56+ phenotype and associated with the Epstein-Barr virus. *Br J Haematol.* 1998;103(3):669-677.
11. Naoe T, Akao Y, Yamada K, et al. Cytogenetic characterization of a T-cell line, ATN-1, derived from adult T-cell leukemia cells. *Cancer Genet Cytogenet.* 1988;34(1):77-88.
12. Gillis S, Watson J. Biochemical and biological characterization of lymphocyte regulatory molecules. V. Identification of an interleukin 2-producing human leukemia T cell line. *J Exp Med.* 1980;152(6):1709-1719.
13. Seto M, Yamamoto K, Iida S, et al. Gene rearrangement and overexpression of PRAD1 in lymphoid malignancy with t(11;14)(q13;q32) translocation. *Oncogene.* 1992;7(7):1401-1406.
14. Moreau EJ, Langerak AW, van Gastel-Mol EJ, et al. Easy detection of all T cell receptor gamma (TCRG) gene rearrangements by Southern blot analysis: recommendations for optimal results. *Leukemia.* 1999;13(10):1620-1626.
15. Ohshima K, Jaffe ES, Kikuchi M. Adult T-cell leukaemia/lymphoma. In: The National Agency for Research on Cancer, Swerdlow S, Campo E, Lee Harris N, et al, eds. *WHO Classification of Tumours of Haematopoietic and Lymphoid Tissues.* Lyon: World Health Organization; 2008: 281-284.
16. Shinawi M, Erez A, Shardy DL, et al. Syndromic thrombocytopenia and predisposition to acute myelogenous leukemia caused by constitutional microdeletions on chromosome 21q. *Blood.* 2008;112(4):1042-1047.
17. Tsukasaki K, Krebs J, Nagai K, et al. Comparative genomic hybridization analysis in adult T-cell leukemia/lymphoma: correlation with clinical course. *Blood.* 2001;97(12):3875-3881.
18. Siegelman MH, Cleary ML, Warnke R, Sklar J. Frequent biclonality and Ig gene alterations among B cell lymphomas that show multiple histologic forms. *J Exp Med.* 1985;161(4):850-863.
19. Takeshita M, Akamatsu M, Ohshima K, et al. CD30 (Ki-1) expression in adult T-cell leukaemia/lymphoma is associated with distinctive immunohistological and clinical characteristics. *Histopathology.* 1995;26(6):539-546.

Overexpression of enhancer of zeste homolog 2 with trimethylation of lysine 27 on histone H3 in adult T-cell leukemia/lymphoma as a target for epigenetic therapy

Daisuke Sasaki,[1] Yoshitaka Imaizumi,[2] Hiroo Hasegawa,[1] Akemi Osaka,[1] Kunihiro Tsukasaki,[2] Young Lim Choi,[3] Hiroyuki Mano,[3] Victor E. Marquez,[4] Tomayoshi Hayashi,[5] Katsunori Yanagihara,[1] Yuji Moriwaki,[2] Yasushi Miyazaki,[2] Shimeru Kamihira,[1] and Yasuaki Yamada[1]

[1]Department of Laboratory Medicine, Nagasaki University Graduate School of Biomedical Sciences, Nagasaki, Japan; [2]Department of Hematology and Molecular Medicine, Atomic Bomb Disease Institute, Nagasaki University Graduate School of Biomedical Sciences, Nagasaki, Japan; [3]Division of Functional Genomics, Jichi Medical University, Tochigi, Japan; [4]Chemical Biology Laboratory, National Cancer Institute, Frederick, MD, USA; and [5]Department of Pathology, Nagasaki University Hospital, Nagasaki, Japan

ABSTRACT

Background
Enhancer of zeste homolog 2 is a component of the Polycomb repressive complex 2 that mediates chromatin-based gene silencing through trimethylation of lysine 27 on histone H3. This complex plays vital roles in the regulation of development-specific gene expression.

Design and Methods
In this study, a comparative microarray analysis of gene expression in primary adult T-cell leukemia/lymphoma samples was performed, and the results were evaluated for their oncogenic and clinical significance.

Results
Significantly higher levels of Enhancr of zeste homolog 2 and RING1 and YY1 binding protein transcripts with enhanced levels of trimethylation of lysine 27 on histone H3 were found in adult T-cell leukemia/lymphoma cells compared with those in normal $CD4^+$ T cells. Furthermore, there was an inverse correlation between the expression level of Enhancer of zeste homolog 2 and that of miR-101 or miR-128a, suggesting that the altered expression of the latter miRNAs accounts for the overexpression of the former. Patients with high Enhancer of zeste homolog 2 or RING1 and YY1 binding protein transcripts had a significantly worse prognosis than those without it, indicating a possible role of these genes in the oncogenesis and progression of this disease. Indeed, adult T-cell leukemia/lymphoma cells were sensitive to a histone methylation inhibitor, 3-deazaneplanocin A. Furthermore, 3-deazaneplanocin A and histone deacetylase inhibitor panobinostat showed a synergistic effect in killing the cells

Conclusions
These findings reveal that adult T-cell leukemia/lymphoma cells have deregulated Polycomb repressive complex 2 with over-expressed Enhancer of zeste homolog 2, and that there is the possibility of a new therapeutic strategy targeting histone methylation in this disease.

Key words: adult T-cell leukemia/lymphoma, human T-cell leukemia virus type-1, Enhancer of zeste homolog 2, H3K27me3.

Citation: Sasaki D, Imaizumi Y, Hasegawa H, Osaka A, Tsukasaki K, Choi YL, Mano H, Marquez VE, Hayashi T, Yanagihara K, Moriwaki Y, Miyazaki Y, Kamihira S, and Yamada Y. Overexpression of enhancer of zeste homolog 2 with trimethylation of lysine 27 on histone H3 in adult T-cell leukemia/lymphoma as a target for epigenetic therapy Haematologica 2011;96(4):712-719. doi:10.3324/haematol.2010.028605

Funding: supported in part by a Grant-in-Aid for Scientific Research from the Ministry of Health, Labour, and Welfare of Japan (N. 04010119). For VEM, this research was supported in part by the Intramural Research Program of the NIH, Center for Cancer Research, NCI-Frederick.

Acknowledgments: the authors thank Sayaka Mori and Yuko Doi for excellent technical assistance.

Manuscript received June 16, 2010. Revised version arrived on December 16, 2010. Manuscript accepted on December 31, 2010.

Correspondence:
Yasuaki Yamada, Department of Laboratory Medicine, 1-7-1 Sakamoto, Nagasaki 852-8501, Japan. Phone: international +81.958197408.
Fax: international +81.958197422.
E-mail: y-yamada@nagasaki-u.ac.jp

The online version of this article has a Supplementary Appendix.

Introduction

The Polycomb group (PcG) proteins play critical roles in the regulation of development by repressing specific sets of developmental genes through chromatin modification.[1] They form two distinct multimeric complexes, Polycomb repressive complex 1 (PRC1) and PRC2, which bind to polycomb responsive elements (PRE), repress genes required for cell differentiation, and maintain pluripotency and self-renewal of embryonic stem cells and hematopoietic stem cells.[2,3] PRC2 consists of Enhancer of zeste homolog 2 (EZH2), which has histone methyltransferase activity, suppressor of zeste 12 (SUZ12), and embryonic ectoderm development (EED), which is required to maintain the integrity of PRC2.[1,4] Sequence-specific DNA binding protein YY1, which recognizes PRE, interacts with EED and recruits PRC2 to a specific chromatin domain to be repressed.[5] EED interacts with histone deacetylase (HDAC) proteins, HDAC1 and HDAC2, and the histone binding proteins RBBP4 (RbAp48) and RBBP7 (RbAp46).[6] PRC2 thus also participates in histone deacetylation. EZH2, as a part of the PRC2 complex, not only methylates histone but also serves as a recruitment platform for DNA methyltransferases that methylate the promoter regions of target genes, which is another mechanism of gene repression.[7] The more diverse complex PRC1 consists of HPC family proteins that mediate chromatin association, HPH family proteins, RING, BMI1, and others.[1] PRC2 initiates trimethylation of lysine 27 on histone H3 (H3K27me3) and, to a lesser extent, lysine 9 of histone H3.[8] PRC1 recognizes H3K27me3 through the chromodomain of the HPC and maintains the trimethylation. There are a number of reports indicating that such epigenetically mediated transcriptional silencing is associated with cancer development.[1,9] Among these, oncogenic roles of over-expressed EZH2 have been studied in a variety of tumors.[10]

Adult T-cell leukemia/lymphoma (ATL) is a neoplasm of mature CD4+ T-cell origin, etiologically associated with human T-cell leukemia virus type-1 (HTLV-1).[11,12] Its clinical behavior differs among patients and is subclassified into four subtypes: smoldering type and chronic type as indolent subtypes, and acute type and lymphoma type as aggressive subtypes.[13] Inactivation of tumor suppressor genes is one of the key events in development and progression, and there is a strong accumulation of *p14ARF/p15INK4B/p16INK4A* gene deletion/methylation or *p53* gene mutations in aggressive subtypes (>60%).[14-20] In the present study, for further investigation of the oncogenesis of ATL, we performed a comparative microarray analysis of gene expression in primary ATL samples. ATL cells expressed significantly higher levels of *EZH2* and *RYBP* (RING1 and YY1 binding protein) transcripts than CD4+ T cells from healthy volunteers. Moreover, acute-type ATL cells showed significantly higher levels of these transcripts than chronic-type ATL cells, suggesting that deregulation of PcG proteins plays a crucial role not only in the development but also in the progression of ATL. In addition, ATL samples were strongly positive for H3K27me3, and were sensitive to 3-deazaneplanocin A (DZNep), a histone methylation inhibitor.[21-23] It has recently been shown that HDAC inhibitor panobinostat (PS, also known as LBH589) depletes the levels of EZH2, SUZ12, and EED and induces apoptotic death in leukemia cells.[24] Deregulation of PcG protein genes with over-expressed EZH2 in ATL cells suggests that ATL is one of the appropriate target diseases for such epigenetic therapy.

Design and Methods

Sample preparation

This study was approved by the ethics committees of Nagasaki University, and all clinical samples were obtained after written informed consent was provided. The diagnosis of ATL was confirmed by the monoclonal integration of HTLV-1 proviral DNA in the genomic DNA of leukemia cells. Peripheral blood mononuclear cells (PBMCs) were obtained from ATL patients (acute type 22 cases, chronic type 19 cases) and healthy adult volunteers by density gradient centrifugation using Lympho-prep (AXIS SHIELD, Oslo, Norway). For enrichment of ATL cells, CD4+ cells were purified from the PBMCs by the magnetic bead method (CD4 MicroBeads, Miltenyi Biotec, Auburn, CA, USA) as described elsewhere.[25] Besides these samples for microarray analysis, we prepared another set of samples for quantitative real-time RT-PCR (qRT-PCR) and Western blotting (25 ATL patients, 13 HTLV-1 carriers, and 12 healthy adults) to confirm the results of microarray analysis. We also used formalin-fixed, paraffin-embedded lymph nodes from 7 patients with lymphoma-type ATL and 5 patients with follicular lymphoma for immunohistochemical analysis.

ATL cell lines used in this study, SO4, ST1, KK1, KOB, and LM-Y1, were established from respective patients in our laboratory and have been confirmed to be of primary ATL cell origin.[26] Cells were maintained in RPMI1640 medium supplemented with 10% FBS and 100 Japan reference units of recombinant interleukin-2 (rIL-2) (kindly provided by Takeda Pharmaceutical Company, Ltd., Osaka, Japan). We also used HTLV-1-infected T-cell lines MT2 and HuT102 and acute T-lymphoblastic leukemia cell lines Jurkat and MOLT4, which were maintained without rIL-2.

DNA microarray analysis

RNA was prepared from purified CD4+ T cells, and subjected to hybridization to HGU133A & B microarray containing 44,760 probe sets for human genes (Affymetrix, Santa Clara, CA, USA) as described previously.[25,27] The mean expression intensity of the internal positive control probe sets (*http://www.affymetrix.com/support/technical/mask_files.affx*) was set to 500 units in each hybridization, and the fluorescence intensity of each test gene was normalized accordingly. All HGU133A & B microarray data are available from the Gene Expression Omnibus website (*http://www.ncbi.nlm.nih.gov/geo*) under the accession number GSE1466.

Quantitative real-time RT-PCR

For confirmation of the results of microarray analysis, we performed quantitative real-time RT-PCR (qRT-PCR) for PcG protein genes. Total RNA was prepared using Isogen (Wako, Osaka, Japan). After removal of contaminated DNA with DNase (Message Clean kit; GenHunter, Nashville, TN, USA), cDNA was constructed from 1 μg of total RNA using the SuperScript III RT-PCR System (Invitrogen, Carlsbad, CA, USA) according to the manufacturer's instructions. Primers and TaqMan probes labeled with TAMRA dye at the 3' end and FAM at the 5' end are listed in *Online Supplementary Table S1*. The mRNA levels for PcG family proteins and porphobilinogen deaminase (PBGD) were measured from a cDNA template using a LightCycler480 PCR System (Roche Diagnostics, Mannheim, Germany). Briefly, reactions were performed in a 20 μL volume with 5 μL (25 ng) of cDNA, 0.5 μM PCR primers, 0.1 μM TaqMan probes, and 10 μL of LightCycler

480 probes Master Mix (Roche Diagnostics). The PCR program consisted of 95°C for 5 min followed by 50 cycles of 95°C for 10 sec and 60°C for 30 sec. After 50 cycles, the absolute amounts of PcG protein mRNA and *PBGD* mRNA were interpolated from the standard curves generated by the dilution method using plasmids derived from a clone transfected with pTAC-1 Vector (BioDynamics Laboratory Inc., Tokyo, Japan) containing amplicons from the PcG family protein and PBGD genes, respectively. To normalize these results for variability in concentration and integrity of RNA and cDNA, the *PBGD* gene was used as an internal control in each sample.

For the quantitative PCR for microRNAs (miRNAs), miR-101, miR-26a, and miR-128a, 10 ng of total RNA (containing miRNA) was used. RT reaction and real-time quantification were performed using TaqMan MicroRNA RT kit and TaqMan MicroRNA assays (hsa-miR-26a, assay ID 000405; hsa-miR-101, assay ID 002253; hsa-miR-128a, assay ID 002216; RNU6B, assay ID 001093) (Applied Biosystems, Foster City, CA, USA) in accordance with the manufacturer's instructions. Each PCR reaction mixture contained 10 μL of LightCycler 480 probes Master Mix, 4 μL of nuclease-free water, 1 μL of 20X specific PCR primer, and 5 μL of RT product. The thermal cycler was programmed as follows: 95°C for 5 min, 40 cycles of 95°C for 15 sec, and 60°C for 60 sec. Using the comparative CT method, we used an endogenous control (RNU6B) to normalize the expression levels of target micro-RNA by correcting differences in the amount of RNA loaded into qPCR reactions.

Western blot analysis and antibodies

Western blot analysis was performed as described previously.[28] The analysis was performed using antibodies to EZH2 and Histone H3 (Cell Signaling Technology, Danvers, MA, USA), phospho EZH2 (Ser21) (Bethyl Laboratories, Montgomery, TX, USA), H3K27me3, dimethylated H3K27 (H3K27me2), monomethylated H3K27 (H3K27me1) (Millipore, Temecula, CA, USA), and β-actin (Sigma, St. Louis, MO, USA).

Immunohistochemistry

Immunohistochemical staining for EZH2 and H3K27me3 was performed on formalin-fixed, paraffin-embedded lymph node samples from lymphoma-type ATL patients and follicular lymphoma patients as a control. The deparaffinized slides were pretreated with DAKO Target Retrieval Solution, pH 9 (DAKO Japan, Tokyo, Japan), and heated in a water bath at 95°C for 40 min. For all stains, the endogenous peroxidase was quenched using 3% H_2O_2 for 15 min. Sections were then placed in 0.5% non-fat dry milk for 30 min at room temperature. The primary antibodies used were anti-EZH2 antibody (BD Biosciences, San Jose, CA, USA) and anti-H3K27me3 antibody (Cell Signaling Technology, Boston, MA, USA), and were applied at 1:50 dilution and 1:100 dilution, respectively. They were allowed to react for 1 h at room temperature, and then the DAKO EnVision™ + Dual Link System-HRP (DAKO Japan, Tokyo, Japan) was applied using diaminobenzidine as the chromogen, following the manufacturer's protocol.

Sensitivity of adult T-cell leukemia/lymphoma cell lines to DZNep and PS (LBH589)

DZNep was synthesized by one of the authors (VEM). Cells were treated with different concentrations of DZNep for 72 h and the cell proliferation status was evaluated by an MTS assay using a Cell Titer 96® AQueos Cell Proliferation Assay kit (Promega, Madison, WI, USA) in accordance with the manufacturer's instructions. To analyze the synergistic effect of combined treatment with DZNep and PS (LBH589) (kindly provided by Novartis Pharma AG, Basel, Switzerland), cells were treated with DZNep (0.3-5.0 μM) and PS (LBH589) (3-50 nM) for 48 h. After the cell proliferation status was evaluated by an MTS assay, the combination index (CI) for each drug combination was obtained by determining the median dose effect of Chou and Talalay using the CI equation within the commercially available software Calcusyn (Biosoft).[29] CI<1, CI=1, and CI>1 indicate synergism, additive effect, and antagonism, respectively. Cell viability represents the value relative to that of the control culture without these agents.

Results

Microarray analysis shows increased EZH2 and/or RYBP transcripts in adult T-cell leukemia/lymphoma cells

In a comparative microarray analysis of primary ATL samples, we focused on investigating PcG protein genes, *EZH2*, *RYBP*, *BMI-1*, and *CBX7*, in the present study because ATL cells show many aberrantly hypermethylated DNA sequences.[30] ATL cells expressed significantly higher levels of *EZH2* and *RYBP* transcripts than $CD4^+$ T cells from healthy adults (Figure 1A and B). In addition, there was a difference between ATL subtypes in these expressions, and cells from the acute type showed significantly higher levels of these transcripts than the cells from the chronic type. When patients were separated into two groups consisting of those with high expression and those with low expression, the group with high *EZH2* or high *RYBP* transcript showed significantly shorter survival than the respective low-expression groups (Figure 1E and F), indicating that high *EZH2* and/or *RYBP* expression is associated with aggressive clinical behavior. Convincingly, there was a trend toward accumulation of acute-type ATL in the high *EZH2* or the high *RYBP* expression group: 14 cases of acute type and 6 cases of chronic type in the high *EZH2* group, 7 cases of acute type and 13 cases of chronic type in the low *EZH2* group, 14 cases of acute type and 6 cases of chronic type in the high RYBP group, and 7 cases of acute type and 13 cases of chronic type in the low RYBP group. BMI1 is known to down-regulate the expression of *p14ARF/p16INK4A* and lead to neoplastic transformation.[31] Chromobox 7 (CBX7), a component of the PRC1, is also known to repress the transcription of *p14ARF/p16INK4A*.[32] Since inactivation of *p14ARF/p15INK4B/p16INK4A* genes is one of the key events in ATL progression, expression of *BMI-1* and/or *CBX7* transcript was expected to be elevated in acute-type ATL cells. There was, however, no difference in these expressions between ATL subtypes or even between ATL cells and normal $CD4^+$ T cells (Figure 1C and D). There was no difference in survival for different *BMI-1* or *CBX7* expression levels (Figure 1G and H).

Confirmation of increased EZH2 and/or RYBP transcripts by quantitative real-time RT-PCR

For confirmation of the results of microarray analysis, we quantified the transcripts of the PcG protein genes including *EZH2* and *RYBP* by qRT-PCR using another set of samples from ATL patients, healthy adults, HTLV-1 carriers, and hematologic cell lines including ATL cell lines. In accordance with the results of microarray analysis, *EZH2* and *RYBP* transcripts were increased in primary ATL cells compared with those in the cells from healthy adults and HTLV-1 carriers, with statistically significantly higher val-

ues in *EZH2* in terms of both absolute copy number per 25 ng of total RNA and normalized expression level (*Online Supplementary Figure S1A, a, B, b*). *RBBP4* was significantly higher in primary ATL cells than in the cells from healthy adults and HTLV-1 carriers in terms of normalized expression level (*Online Supplementary Figure S1 C, c*). In contrast, there was no difference in *BMI1*, *YY1*, and *EED* expressions among these groups, although some patients showed very high *BMI1* expression (*Online Supplementary Figure S1D, d, E, e, F, f*). Similarly to primary ATL cells, some ATL cell lines showed high *EZH2* expression in terms of absolute copy number per 25 ng of total RNA (*Online Supplementary Figure S1A*).

EZH2 protein expression with trimethylation of H3K27 is characteristic in adult T-cell leukemia/lymphoma cells

We then examined EZH2 and RYBP at the protein level by Western blotting. A 98-kDa band for EZH2 protein and a 32-kDa band for RYBP protein were detected in all primary ATL samples irrespective of subtype, but they were hardly detected in cells from healthy adults and HTLV-1 carriers (Figure 2A, *Online Supplementary Figure S2*, and *data not shown*). ATL cell lines and acute T-lymphoblastic leukemia cell lines also showed intense EZH2 bands. The serine-threonine kinase Akt phosphorylates EZH2 at serine 21 and suppresses its methyltransferase activity by impeding EZH2 binding to histone H3, which results in a decrease in lysine 27 trimethylation.[33] EZH2 of ATL cells was not phosphorylated and was in its active form (Figure 2A). In fact, most primary ATL samples showed the band for H3K27me3, while the cells from healthy adults lacked the band (Figure 2B). As it is known that EZH2 plays a crucial role in trimethylation but not in dimethylation or monomethylation, the bands for H3K27me2 and H3K27me1 were detected in all samples examined, but the band for H3K27me3 was limited in primary ATL cells and ATL cell lines LMY1 and KOB that showed an intense EZH2 band with a faint phosphorylated EZH2 band (Figure 2A and B). In contrast, EZH2 was strongly phosphorylated in ATL cell lines ST1, SO4, KK1, and acute T-lymphoblastic leukemia cell lines Jurkat and MOLT4, and these cell lines hardly showed the band for H3K27me3. Collectively, these results indicate that ATL cells express

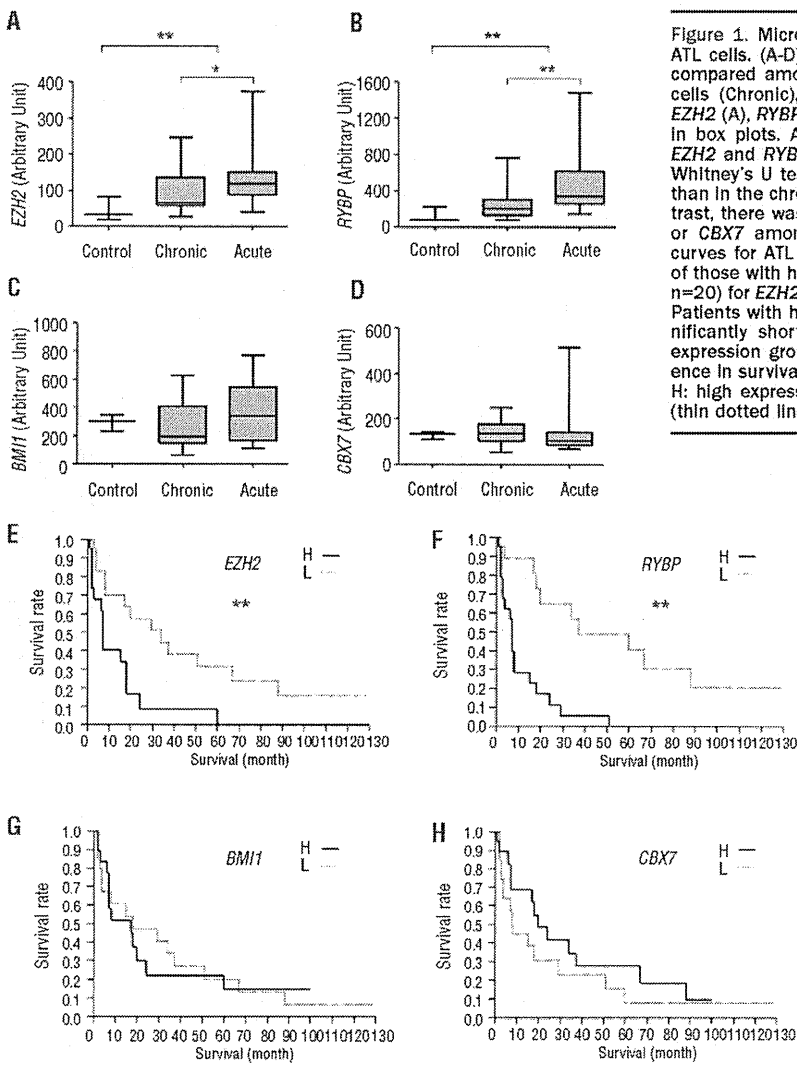

Figure 1. Microarray analysis of gene expression in primary ATL cells. (A-D) Expression levels of PcG protein genes were compared among normal CD4+ T cells (Control), chronic ATL cells (Chronic), and acute ATL cells (Acute), and results of *EZH2* (A), *RYBP* (B), *BMI1* (C), and *CBX7* (D) are demonstrated in box plots. ATL cells showed significantly higher levels of *EZH2* and *RYBP* transcripts than normal CD4+ T cells (Mann-Whitney's U test), with a higher expression in the acute type than in the chronic type (Mann-Whitney's U test) (A, B). In contrast, there was no statistical difference in the level for *BMI1* or *CBX7* among these groups (C, D). (E-H) Overall survival curves for ATL patients separated into two groups consisting of those with high expression (H, n=20) and low expression (L, n=20) for *EZH2* (E), *RYBP* (F), *BMI1* (G), or *CBX7* (H) are shown. Patients with high *EZH2* or high *RYBP* expression showed significantly shorter survival than those in corresponding low expression groups (log rank test) (E, F). There was no difference in survival for different *BMI1* or *CBX7* expressions (G, H). H: high expression group (bold line), L: low expression group (thin dotted line). $*P<0.05$, $**P<0.01$

functionally active EZH2, and as a result, their H3K27 are trimethylated, and that ATL cell lines LMY1 and KOB preserve this characteristic of primary ATL cells.

Immunohistochemical confirmation of the expression of EZH2 and H3K27me3 in lymph nodes

We next used lymph nodes from lymphoma-type ATL patients for immunohistochemical evaluation of EZH2 expression and H3K27me3. In agreement with the results of Western blotting, all ATL lymph nodes from 7 patients were strongly positive for both EZH2 and H3K27me3 without exception in their nuclear staining (*Online Supplementary Figure S3* and *data not shown*), suggesting that overexpression of EZH2 with H3K27me3 is a common feature of ATL cells irrespective of ATL subtypes. In contrast, in lymph nodes from 5 follicular lymphoma patients, only a few cells were positive for EZH2 with some variation among patients and most cells were negative for H3K27me3 (*Online Supplementary Figure S3* and *data not shown*).

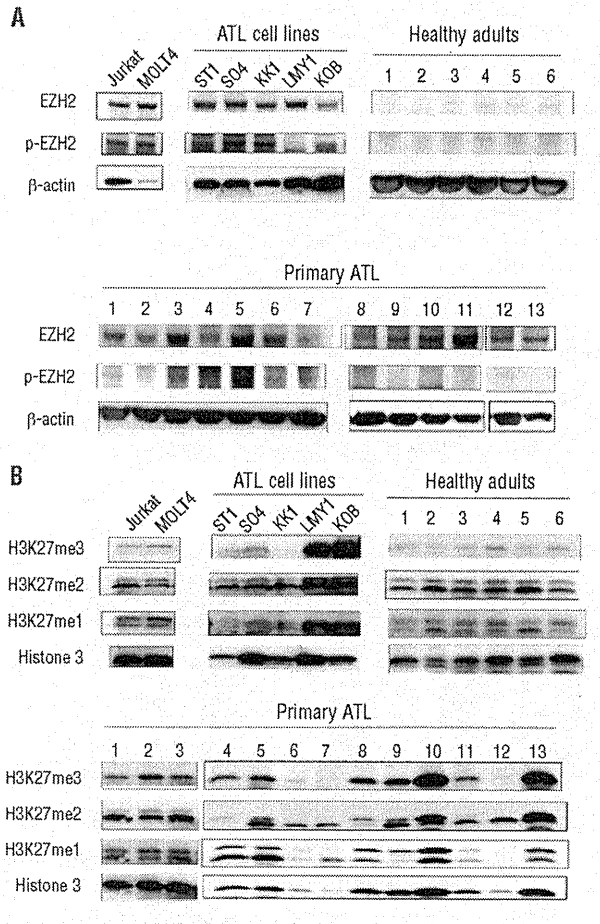

Figure 2. EZH2 protein expression and histone methylation. (A) Western blot analysis for EZH2 protein was performed on primary ATL cells, cells from healthy adults, and ATL cell lines. Primary ATL cells showed a clear 98-kDa band for EZH2 with the absence or presence of faint bands for phosphorylated EZH2 (p-EZH2). Cells from healthy adults hardly showed these bands. ATL cell lines ST1, SO4, and KK1 showed intense bands for both EZH2 and p-EZH2, but LM-Y1 and KOB cells showed intense bands for EZH2 with the absence of a band for p-EZH2. (B) Western blot analysis for histone methylation status was performed. Only primary ATL cells and LM-Y1 and KOB cell lines showed a clear band for H3K27me3, but others hardly showed the band. Bands for H3K27me2, H3K27me1, and histone H3 were observed in almost all samples examined.

Downregulation of miR-101 and miR-128a may be responsible for increased EZH2 expression

So far, more than 700 miRNAs have been identified in humans, and each miRNA regulates multiple target genes. miR-101 and miR-26a have been shown to be negative regulators of *EZH2* expression and are depressed in several types of cancer cells.[34,35] miR-128a is known to be a negative regulator of *BMI1* and has been reported to be involved in glioma cell proliferation.[36] We quantified these miRNAs in primary ATL cells and cells from HTLV-1 carriers to investigate the mechanism of *EZH2* overexpression. ATL cells showed significantly decreased levels of miR-101 and miR-128a compared with the cells from HTLV-1 carriers (Figure 3A and C). Notably, there were significant inverse correlations between *EZH2* expression and miR-101 expression or *EZH2* expression and miR-128a expression (Figure 3D and E), suggesting that decrease of these miRNAs accounts for the overexpression of *EZH2*. Since genomic loss of miR-101 has been reported in prostate cancer,[34] we performed quantitative genomic PCR for miR-101 in two loci, miR-101-1 (chromosome 1p31) and miR-101-2 (chromosome 9p24). Both loci were preserved in all 10 ATL samples examined (*Online Supplementary Figure S4*). The expression of miR-26a did not, in contrast, differ between ATL cells and cells from HTLV-1 carriers (Figure 3B). Unexpectedly, there was no significant correlation between *BMI1* expression and miR-128a expression (Figure 3F).

Adult T-cell leukemia/lymphoma cells are sensitive to DZNep and PS (LBH589)

We first examined the sensitivity of ATL-related cell lines and acute T-lymphoblastic leukemia cell lines to DZNep, an inhibitor of S-adenosylhomocysteine hydrolase, which has recently been shown to decrease the expression of EZH2 and histone methylation.[22,23] DZNep inhibited the proliferation of these cell lines, at concentrations above 0.5 μM (*Online Supplementary Figure S5A*). In contrast, $CD4^+$ T cells from healthy adults as a normal control were resistant to DZNep even at 5 μM. Notably, although DZNep decreased *EZH2* expression in ST1, SO4, and KK1, it did not decrease but rather increased the expression in KOB, results which were confirmed by Western blot (*Online Supplementary Figure S5B and C*). PS (LBH589) is also known to decrease the level of EZH2 in several types of leukemia cells.[24] One hundred nM of PS (LBH589) decreased *EZH2* expression at both transcript and protein levels in ATL cell lines including KOB and LM-Y1, which showed a similar EZH2 expression profile to that of primary ATL cells, namely, high EZH2 expression with low phosphorylated EZH2 and strong H3K27me3 (*Online Supplementary Figure S5D and E*). We next examined whether these agents show a synergistic effect or just an additive effect. As shown in *Online Supplementary Figure S5F* (upper panel), the cell viabilities of LM-Y1 treated with 25 nM PS (LBH589) or 2.5 μM DZNep were 70% and 87%, respectively. A combination of this setting (LBH:DZNep=1:100) markedly decreased the proportion of viable cells (40%) compared with that of cells treated

with either agent alone. Similarly, cell viabilities of KOB treated with 25 nM PS (LBH589), 2.5 μM DZNep, or a combination of these agents were 86%, 93%, and 48%, respectively. By calculating CI according to the method of Chou and Talalay,[29] we found a strong synergistic antiproliferative effect in both cell lines (*Online Supplementary Figure S5F*, lower panel).

Discussion

EZH2 is a critical component of PRC2, which mediates epigenetic gene silencing through trimethylation of H3K27.[37,39] EED and SUZ12 are also required for the exhibition of methyltransferase activity and for the localization of this complex to target genes.[39] In an analysis of genome-wide H3K27 methylation in aggressive prostate cancer tissues, a significant subset of the target genes were also targets in embryonic stem cells, suggesting that the mechanism for gene silencing used to maintain stem cell renewal is converted into oncogenesis.[40] Ectopic expression of EZH2 is capable of providing a proliferative advantage to primary cells, and its gene locus is amplified in primary tumors.[41] Indeed, increased EZH2 expression has been reported in several types of cancer cells, and its clinical significance is extensively studied in prostate cancer.[42] Amounts of both *EZH2* transcript and EZH2 protein were elevated in metastatic prostate cancer; in addition, clinically localized prostate cancers that express higher concentrations of *EZH2* showed a poorer prognosis. An association of increased EZH2 expression with poor prognosis has also been reported in other solid tumors. Currently, however, there are only limited reports describing EZH2 expression in hematologic malignancies.

In the present study, we showed for the first time that EZH2 was over-expressed in ATL cells, and that the increased EZH2 was not phosphorylated and was in its active form. The increased EZH2 seemed to exhibit histone methyltransferase activity *in vivo*, as supported by the results that ATL cells from both peripheral blood and lymph nodes were strongly positive for H3K27me3. Since EZH2 was almost undetectable in cells from healthy adults and HTLV-1 carriers, it is likely that deregulation of PRC2 caused by over-expressed EZH2 is involved in the early steps of ATL oncogenesis. Meanwhile, ATL patients with high EZH2 expression showed shorter survival than patients with low EZH2 expression, indicating that increased EZH2 also plays a role in the process of ATL progression. It has been reported that genes methylated in cancer cells are specifically packaged with nucleosomes containing H3K27.[43] However, there are only a few studies that actually examined H3K27me3 in primary tumor cells or tissues. In one such study, H3K27me3 expression was unexpectedly lower in breast, ovarian, and pancreatic cancers than in corresponding normal tissues, although it has been reported that there are increased levels of H3K27me3 in breast cancer cell lines.[44,45] We do not have an adequate explanation for these conflicts at present, but there may be some differences in the process of oncogenesis between solid tumors and hematologic malignancies.

The mechanism of the overexpression of EZH2 in tumors remains largely unknown. miRNAs regulate gene expression and play important roles in cellular differentiation and embryonic stem cell development. Recently, two miRNAs, miR-101 and miR-26a, were found to repress *EZH2* expression. The expression of miR-101 decreases in parallel with an increase in *EZH2* expression during progression in prostate tumors.[34] In addition to these miRNAs, we examined miR-128a, which has been shown to repress *BMI1* expression in glioblastoma, because overexpression of *BMI-1* is associated with the development of malignant lymphoma.[31,36] ATL cells showed a decreased level of miR-

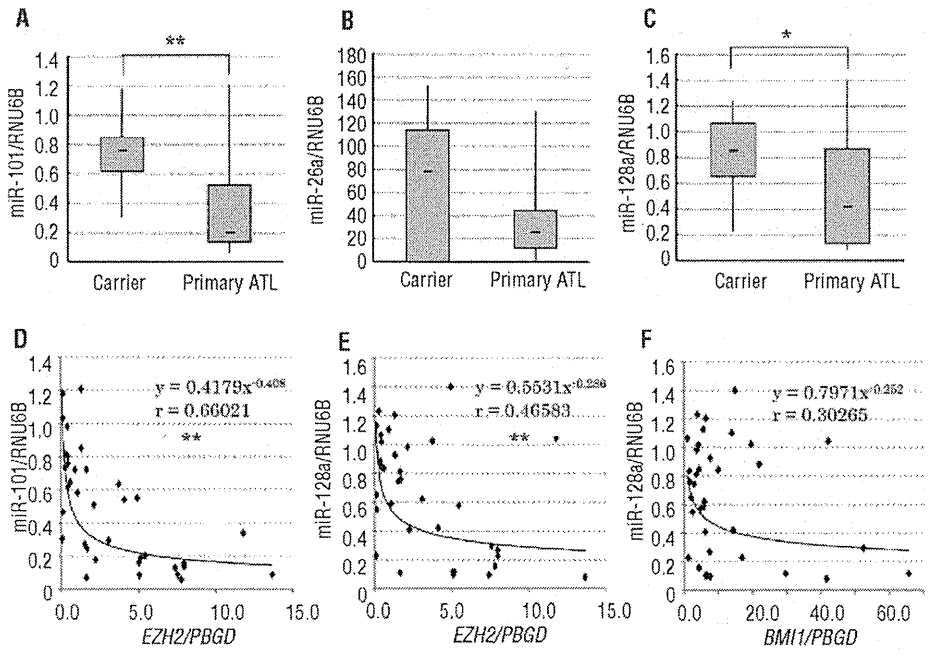

Figure 3. Quantitative real-time RT-PCR for miRNAs. (A-C) Expressions of miR-101 (A), miR-26a (B), and miR-128a (C) were compared between ATL patients and HTLV-1 carriers. Primary ATL cells showed significantly lower levels of miR-101 and miR-128a (Mann-Whitney's U test) compared with the cells from HTLV-1 carriers (A, C). There was no significant difference in miR-26a expression between the two groups (B). (D, E, F) Correlation between miRNA and *EZH2* or *BMI1* expression was examined. There were significant inverse correlations between normalized *EZH2* expression and miR-101 expression (D) or between normalized *EZH2* expression and miR-128a expression (E) (Spearman's correlation coefficient). In contrast, there was no correlation between normalized *BMI1* expression and miR-128a expression (F). $*P<0.05$, $**P<0.01$

101 expression compared with the cells from HTLV-1 carriers, which is not caused by genomic loss of the *miR-101* gene, in contrast to prostate cancer.[34] Moreover, there was a clear inverse correlation between *EZH2* expression and miR-101 expression, suggesting that increased *EZH2* is caused by the decrease in miR-101 expression. Although currently there is no report indicating an association of miR-128a with *EZH2* expression, miR-128a showed exactly the same pattern as miR-101, suggesting that the decrease in miR-128a also participates in *EZH2* overexpression in ATL. By analyzing the 3'-UTR sequence of *EZH2*, it has recently been shown that there are two predicted miR-101 target sites and one predicted miR-26a target site in the 3'-UTR of EZH2.[46] We performed a similar analysis and found that there was also a potential target site for miR-128a near one of the miR-101 target sites (*Online Supplementary Figure S6*). miR-26a was not decreased in ATL cells, and there was no correlation between miR-26a expression and *EZH2* expression or miR-128a expression and *BMI1* expression. The association of miR-26a with *EZH2* was found in normal cell differentiation as a physiological phenomenon but not in tumor cells. The miRNAs used to regulate normal development and differentiation may be different from those used for the development of tumors. Another possible explanation for the mechanism of increased *EZH2* expression in ATL is inactivation of *p14ARF/p15INK4B/p16INK4A* tumor suppressor genes, which frequently occurs in ATL.[14,15,19,20] EZH2 is a molecule downstream of the pRB-E2F pathway, and inactivation of these genes allows E2F to be released from pRB, which results in the upregulation of *EZH2* expression.[41] Several recent reports indicate that EZH2 functions to repress the expression of *p14ARF/p15INK4B/p16INK4A*; therefore, increased EZH2 may be used to further decrease the expression of *p14ARF/p15INK4B/p16INK4A*.[47] Since somatic mutations altering EZH2 (Tyr641) have recently been reported in follicular and diffuse large B-cell lymphomas of germinal-center origin,[48] we performed a similar analysis in 10 primary ATL samples. There were however no such mutations (*Online Supplementary Figure S7*).

ATL is quite resistant to antineoplastic agents and the median survival time of those with the aggressive subtypes is only 13 months, even in a recent multicenter clinical trial.[49] Since high EZH2 expression with H3K27me3 seems to be an essential component for the initiation and promotion of cell proliferation in ATL, we searched for the possibility of therapeutic strategies targeting EZH2. We examined the sensitivity of ATL cells to agents that have been shown to inhibit *EZH2* expression and histone methylation. DZNep is a carbocyclic analog of adenosine synthesized more than 20 years ago as an inhibitor of S-adenosylhomocysteine hydrolase, which has therapeutic potential as an anticancer or antiviral drug.[21] DZNep has recently aroused interest for its unique features; it decreases the expressions of *EZH2*, *SUZ12*, and *EED* with inhibition of H3K27 methylation and induces apoptosis in cancer cells but not in normal cells.[22,23] ATL cell lines were sensitive to DZNep and their cell proliferation was attenuated at one-tenth of the concentration used in these studies. More interestingly, DZNep showed no toxicity to normal $CD4^+$ T cells as a normal control. Acute T-lymphoblastic leukemia cell lines showed similar sensitivities to DZNep, which may indicate that DZNep exerts general toxicity to leukemia and lymphoma cells not necessarily associated with histone modification. Indeed, although DZNep rather increased EZH2 expression in KOB cells, this cell line was equally sensitive as other cell lines to DZNep. HDAC inhibitor PS (LBH589) is an effective agent for cutaneous T-cell lymphoma and induced complete remission in 2 of 9 patients involved in a phase I clinical trial.[50] More interestingly, it has been reported recently that combined use of DZNep and PS (LBH589) yielded more depletion of EZH2 and induced more apoptosis of leukemia cells, but not normal CD34 (+) bone marrow progenitor cells.[51] In the present study, we showed that the combination of DZNep and PS (LBH589) exhibited a synergistic effect in killing ATL cells. Thus, epigenetic therapy by the combined use of these agents that inhibit histone methylation could lead to a breakthrough in the treatment of aggressive ATL.

Authorship and Disclosures

The information provided by the authors about contributions from persons listed as authors and in acknowledgments is available with the full text of this paper at www.haematologica.org.

Financial and other disclosures provided by the authors using the ICMJE (www.icmje.org) Uniform Format for Disclosure of Competing Interests are also available at www.haematologica.org.

References

1. Sparmann A, van Lohuizen M. Polycomb silencers control cell fate, development and cancer. Nat Rev Cancer. 2006;6(11):846-56.
2. Lee TI, Jenner RG, Boyer LA, Guenther MG, Levine SS, Kumar RM, et al. Control of developmental regulators by Polycomb in human embryonic stem cells. Cell. 2006;125(2):301-13.
3. Kamminga LM, Bystrykh LV, de Boer A, Houwer S, Douma J, Weersing E, et al. The Polycomb group gene Ezh2 prevents hematopoietic stem cell exhaustion. Blood. 2006;107(5):2170-9.
4. van Lohuizen M, Tijms M, Voncken JW, Schumacher A, Magnuson T, Wientjens E. Interaction of mouse polycomb-group (Pc-G) proteins Enx1 and Enx2 with Eed: Indication for separate Pc-G complexes. Mol Cell Biol. 1998;18(6):3572-9.
5. Satijn DP, Hamer KM, den Blaauwen J, Otte AP. The Polycomb group protein EED interacts with YY1, and both proteins induce neural tissue in Xenopus embryos. Mol Cell Biol. 2001;21(4):1360-9.
6. van der Vlag J, Otte AP. Transcriptional repression mediated by the human polycomb-group protein EED involves histone deacetylation. Nat Genet. 1999;23(4):474-8.
7. Vire E, Brenner C, Deplus R, Blanchon L, Fraga M, Didelot C, et al. The Polycomb group protein EZH2 directly controls DNA methylation. Nature. 2006;439(7078):871-4.
8. Cao R, Zhang Y. The functions of E(Z)/EZH2-mediated methylation of lysine 27 in histoneH3. Curr Opin Genet Dev. 2004;14(2):155-64.
9. Widschwendter M, Fiegl H, Egle D, Mueller-Holzner E, Spizzo G, Marth C, et al. Epigenetic stem cell signature in cancer. Nat Genet. 2007;39(2):157-8.
10. Simon JA, Lange CA. Roles of the EZH2 histone methyltransferase in cancer epigenetics. Mutat Res. 2008;647(1-2):21-9.
11. Uchiyama T, Yodoi J, Sagawa K, Takatsuki K, Uchino H. Adult T-cell leukemia: clinical and hematologic features of 16 cases. Blood. 1977;50(3):481-92.
12. Yoshida M, Seiki M, Yamaguchi K, Takatsuki K. Monoclonal integration of human T-cell leukemia provirus in all primary tumors of adult T-cell leukemia suggests causative role of human T-cell leukemia virus in the disease. Proc Natl Acad Sci USA. 1984;81(8):2534-7.
13. Shimoyama M and members of the Lymphoma Study Group (1984-1987):

Diagnostic criteria and classification of clinical subtypes of adult T-cell leukaemia-lymphoma. A report from the Lymphoma Study Group (1984-1987). Br J Haematol. 1991;79(3):428-37.
14. Hatta Y, Hirama T, Miller CW, Yamada Y, Tomonaga M, Koeffler HP. Homozygous deletions of p15 (MTS2) and p16 (CDKN2/MTS1) genes in adult T-cell leukemia. Blood. 1995;85(10):2699-704.
15. Yamada Y, Hatta Y, Murata K, Sugawara K, Ikeda S, Mine M, et al. Deletions of p15 and/or p16 genes as a poor-prognosis factor in adult T-cell leukemia. J Clin Oncol. 1997;15(5):1778-85.
16. Nagai H, Kinoshita T, Imamura J, Murakami Y, Hayashi K, Mukai K, et al. Genetic alteration of p53 in some patients with adult T-cell leukemia. Jpn J Cancer Res. 1991;82(12):1421-7.
17. Sakashita A, Hattori T, Miller CW, Suzushima H, Asou N, Takatsuki K, et al. Mutations of the p53 gene in adult T-cell leukemia. Blood. 1992;79(2):477-80.
18. Tawara M, Hogerzeil SJ, Yamada Y, Takasaki Y, Soda H, Hasegawa H, et al. Impact of p53 aberration on the progression of adult T-cell leukemia/lymphoma. Cancer Lett. 2006;234(2):249-55.
19. Kohno T, Yamada Y, Tawara M, Takasaki Y, Kamihira S, Tomonaga M, et al. Inactivation of p14ARF as a key event for the progression of adult T-cell leukemia/lymphoma. Leuk Res. 2007;31(12):1625-32.
20. Nosaka K, Maeda M, Tamiya S, Sakai T, Mitsuya H, Matsuoka M. Increasing methylation of the CDKN2A gene is associated with the progression of adult T-cell leukemia. Cancer Res. 2000;60(4):1043-8.
21. Glazer RI, Hartman KD, Knode MC, Richard MM, Chiang PK, Tseng CK, et al. 3-Deazaneplanocin: a new and potent inhibitor of S-adenosylhomocysteine hydrolase and its effects on human promyelocytic leukemia cell line HL-60. Biochem Biophys Res Commun. 1986;135 (2):688-94.
22. Miranda TB, Cortez CC, Yoo CB, Liang G, Abe M, Kelly TK, et al. DZNep is a global histone methylation inhibitor that reactivates developmental genes not silenced by DNA methylation. Mol Cancer Ther. 2009;8(6):1579-88.
23. Tan J, Yang X, Zhuang L, Jiang X, Chen W, Lee PL, et al. Pharmacologic disruption of Polycomb-repressive complex 2-mediated gene repression selectively induces apoptosis in cancer cells. Genes Dev. 2007;21(9): 1050-63.
24. Fiskus W, Pranpat M, Balasis M, Herger B, Rao R, Chinnaiyan A, et al. Histone deacetylase inhibitors deplete EZH2 and associated Polycomb Repressive Complex 2 proteins with attenuation of HOXA9 and MEIS1 and loss of survival of human acute leukemia cells. Mol Cancer Ther. 2006;5 (12):3096-104.
25. Choi YL, Tsukasaki K, O'Neill MC, Yamada Y, Onimaru Y, Matsumoto K, et al. A genomic analysis of adult T-cell leukemia. Oncogene. 2007;26(8):1245-55.
26. Yamada Y, Ohmoto Y, Hata T, Yamamura M, Murata K, Tsukasaki K, et al. Features of the cytokines secreted by adult T cell leukemia (ATL) cells. Leuk Lymphoma. 1996;21(5-6):443-7.
27. Choi YL, Makishima H, Ohashi J, Yamashita Y, Ohki R, Koinuma K, et al. DNA microarray analysis of natural killer cell-type lymphoproliferative disease of granular lymphocytes with purified CD3(-) CD56(+) fractions. Leukemia. 2004;18(3): 556-65.
28. Hasegawa H, Yamada Y, Komiyama K, Hayashi M, Ishibashi M, Sunazuka T, et al. A novel natural compound, a cycloanthranilylproline derivative (Fuligocandin B), sensitizes leukemia cells to apoptosis induced by tumor necrosis factor related apoptosis-inducing ligand (TRAIL) through 15-deoxy-Delta 12, 14 prostaglandin J2 production. Blood. 2007;110(5):1664-74.
29. Chou TC, Talalay P. Quantitative analysis of dose-effect relationships: the combined effects of multiple drugs or enzyme inhibitors. Adv Enzyme Regul. 1984;22:27-55.
30. Yasunaga J, Taniguchi Y, Nosaka K, Yoshida M, Satou Y, Sakai T, et al. Identification of aberrantly methylated genes in association with adult T-cell leukemia. Cancer Res. 2004;64(17):6002-9.
31. Jacobs JJ, Kieboom K, Marino S, DePinho RA, van Lohuizen M. The oncogene and Polycomb-group gene bmi-1 regulates cell proliferation and senescence through the ink4a locus. Nature. 1999;397(6715):164-8.
32. Scott CL, Gil J, Hernando E, Teruya-Feldstein J, Narita M, Martinez D, et al. Role of the chromobox protein CBX7 in lymphomagenesis. Proc Natl Acad Sci USA. 2007;104(13):5389-94.
33. Cha TL, Zhou BP, Xia W, Wu Y, Yang CC, Chen CT, et al. Akt-mediated phosphorylation of EZH2 suppresses methylation of Lysine 27 in histone H3. Science. 2005;310(5746):306-10.
34. Varambally S, Cao Q, Mani RS, Shankar S, Wang X, Ateeq B, et al. Genomic loss of microRNA-101 leads to overexpression of histone methyltransferase EZH2 in cancer. Science. 2008;322(5908):1695-6.
35. Sander S, Bullinger L, Klapproth K, Fiedler K, Kestler HA, Barth TF, et al. MYC stimulates EZH2 expression by repression of its negative regulator miR-26a. Blood. 2008; 112(10):4202-12.
36. Godlewski J, Nowicki MO, Bronisz A, Williams S, Otsuki A, Nuovo G, et al. Targeting of the Bmi-1 oncogene/stem cell renewal factor by microRNA-128 inhibits glioma proliferation and self-renewal. Cancer Res. 2008;68(22):9125-30.
37. Cao R, Wang L, Wang H, Xia L, Erdjument-Bromage H, Tempst P, et al. Role of histone H3 lysine 27 methylation in Polycomb-group silencing. Science. 2002;298(5595): 1039-43.
38. Czermin B, Melfi R, McCabe D, Seitz V, Imhof A, Pirrotta V. Drosophila enhancer of Zeste/ESC complexes have a histone H3 methyltransferase activity that marks chromosomal Polycomb sites. Cell. 2002;111(2): 185-96.
39. Cao R, Zhang Yl. SUZ12 is required for both the histone methyltransferase activity and the silencing function of the EED-EZH2 complex. Mol Cell. 2004;15(1):57-67.
40. Yu J, Yu J, Rhodes DR, Tomlins SA, Cao X, Chen G, et al. A polycomb repression signature in metastatic prostate cancer predicts cancer outcome. Cancer Res. 2007; 67(22):10657-63.
41. Bracken AP, Pasini D, Capra M, Prosperini E, Colli E, Helin K. EZH2 is down stream of the pRB-E2F pathway, essential for proliferation and amplified in cancer. EMBO J. 2003;22(20):5323-35.
42. Varambally S, Dhanasekaran SM, Zhou M, Barrette TR, Kumar-Sinha C, Sanda MG, et al. The polycomb group protein EZH2 is involved in progression of prostate cancer. Nature. 2002;419(6907):624-9.
43. Schlesinger Y, Straussman R, Keshet I, Farkash S, Hecht M, Zimmerman J, et al. Polycomb-mediated methylation of Lys27 of histone H3 pre-marks genes for de novo methylation in cancer. Nat Genet. 2007;39 (2):232-6.
44. Wei Y, Xia W, Zhang Z, Liu J, Wang H, Adsay NV, et al. Loss of trimethylation at lysine 27 of histone H3 is a predictor of poor outcome in breast, ovarian, and pancreatic cancers. Mol Carcinog. 2008;47 (9):701-6.
45. Sun F, Chan E, Wu Z, Yang X, Marquez VE, Yu Q. Combinatorial pharmacologic approaches target EZH2-mediated gene repression in breast cancer cells. Mol Cancer Ther. 2009;8(12):3191-202.
46. Cao P, Deng Z, Wan M, Huang W, Cramer SD, Xu J, et al. MicroRNA-101 negatively regulates Ezh2 and its expression is modulated by androgen receptor and HIF-1alpha/HIF-1beta. Mol Cancer. 2010;9: 108.
47. Bracken AP, Kleine-Kohlbrecher D, Dietrich N, Pasini D, Gargiulo G, Beekman C, et al. The polycomb group proteins bind throughout the INK4A-ARF locus and are disassociated in senescent cells. Genes Dev. 2007;21(5):525-30.
48. Morin RD, Johnson NA, Severson TM, Mungall AJ, An J, Goya R, et al. Somatic mutations altering EZH2 (Tyr641) in follicular and diffuse large B-cell lymphomas of germinal-center origin. Nat Genet. 2010; 42(2):181-5.
49. Yamada Y, Tomonaga M, Fukuda H, Hanada S, Utsunomiya A, Tara M, et al. A new G-CSF-supported combination chemotherapy, LSG15, for adult T-cell leukaemia-lymphoma: Japan Clinical Oncology Group Study 9303. Br J Haematol. 2001;113(2):375-82.
50. Ellis L, Pan Y, Smyth GK, George DJ, McCormack C, Williams-Truax R, et al. Histone deacetylase inhibitor panobinostat induces clinical responses with associated alterations in gene expression profiles in cutaneous T-cell lymphoma. Clin Cancer Res. 2008;14(14):4500-10.
51. Fiskus W, Wang Y, Sreekumar A, Buckley KM, Shi H, Jillella A, et al. Combined epigenetic therapy with the histone methyltransferase EZH2 inhibitor 3-deazaneplanocin A and the histone deacetylase inhibitor panobinostat against human AML cells. Blood. 2009;114(13):2733-43.

Cancer Cell
Article

Polycomb-Mediated Loss of miR-31 Activates NIK-Dependent NF-κB Pathway in Adult T Cell Leukemia and Other Cancers

Makoto Yamagishi,[1,3] Kazumi Nakano,[1] Ariko Miyake,[1] Tadanori Yamochi,[1] Yayoi Kagami,[1] Akihisa Tsutsumi,[1] Yuka Matsuda,[1] Aiko Sato-Otsubo,[4] Satsuki Muto,[1,4] Atae Utsunomiya,[5] Kazunari Yamaguchi,[6] Kaoru Uchimaru,[2] Seishi Ogawa,[4] and Toshiki Watanabe[1,*]
[1]Graduate School of Frontier Sciences
[2]Institute of Medical Science
The University of Tokyo, Tokyo, 108-8639, Japan
[3]Japan Foundation for AIDS Prevention, Tokyo, 101-0061, Japan
[4]Cancer Genomics Project, Graduate School of Medicine, The University of Tokyo, Tokyo, 113-8655, Japan
[5]Department of Haematology, Imamura Hospital, Bun-in, Kagoshima, 890-0064, Japan
[6]Department of Safety Research on Blood and Biologics, NIID, Tokyo, 208-0611, Japan
*Correspondence: tnabe@ims.u-tokyo.ac.jp
DOI 10.1016/j.ccr.2011.12.015

SUMMARY

Constitutive NF-κB activation has causative roles in adult T cell leukemia (ATL) caused by HTLV-1 and other cancers. Here, we report a pathway involving Polycomb-mediated miRNA silencing and NF-κB activation. We determine the miRNA signatures and reveal miR-31 loss in primary ATL cells. MiR-31 negatively regulates the noncanonical NF-κB pathway by targeting NF-κB inducing kinase (NIK). Loss of miR-31 therefore triggers oncogenic signaling. In ATL cells, miR-31 level is epigenetically regulated, and aberrant upregulation of Polycomb proteins contribute to miR-31 downregulation in an epigenetic fashion, leading to activation of NF-κB and apoptosis resistance. Furthermore, this emerging circuit operates in other cancers and receptor-initiated NF-κB cascade. Our findings provide a perspective involving the epigenetic program, inflammatory responses, and oncogenic signaling.

INTRODUCTION

Adult T cell leukemia (ATL) is an aggressive T cell neoplasm with very poor prognosis (Yamaguchi and Watanabe, 2002). Human T cell leukemia virus type I (HTLV-I) is recognized as an etiological factor in T cell malignancy. Although mounting molecular evidence has contributed to our ability to cure several cancers and other diseases, the genetic background of ATL leukemogenesis is not yet fully understood. Thus, it is an urgent request to clarify the molecular mechanism of ATL development.

Constitutive activation of nuclear factor-κB (NF-κB) is observed in the ATL cell lines and primary isolated tumor cells from ATL patients, although the viral oncoprotein Tax, a powerful activator of NF-κB, is not expressed in these malignant cells (Hironaka et al., 2004; Watanabe et al., 2005). NF-κB activation aberrantly contributes to cell propagation and anti-apoptotic responses in ATL and other cancers (Prasad et al., 2010). In our previous study, inhibition of NF-κB activity with a specific inhibitor, DHMEQ, drastically impaired the levels of ATL cell growth and resistance to apoptosis (Watanabe et al., 2005), suggesting that the molecular background of aberrant NF-κB activation may give us potential therapeutic targets. A recent report provided a new readout that NF-κB-inducing kinase (NIK) has a causal role in tumor progression and the aggressive phenotypes of various cancers, including ATL (Saitoh et al., 2008). NIK plays a pivotal role in the noncanonical (alternative) NF-κB pathway as a crucial kinase in receptor-initiating signaling, including signaling from CD40, LTBR, and BAFFR.

Significance

Here, we propose a molecular perspective of the onset of oncogenic signaling. NIK overexpression is a major driving force for constitutive NF-κB activation in various types of cancers. Using ATL cells as a model of NF-κB-addiction, we identified miR-31 as a suppressor of NIK that is completely silenced in ATL cells. Furthermore, an oncogenic function of a subset of Polycomb is implicated in NF-κB signaling via miRNA regulation. This study introduces a fundamental link between the Polycomb-mediated epigenetic regulation and the NF-κB signaling, allowing us to attribute the constitutive activation of NF-κB to epigenetic reprogramming.

Several studies have recently implicated another functional significance of NIK protein in epithelial cell proliferation, inflammatory response, and oncogenic signaling (for review, see Thu and Richmond, 2010). Although the expression level of NIK is strictly maintained by proteasomal degradation in normal cells (Liao et al., 2004), increased level of NIK transcript are observed in some cancers, causing inappropriate accumulation of NIK protein without stimuli (Annunziata et al., 2007; Saitoh et al., 2008). Overexpression of NIK leads to aberrant phenotypes in several cell types; however, little is known about the abnormal accumulation of NIK in malignant cells.

Recent advances have led to deeper understanding of a new aspect of posttranscriptional gene regulation, i.e., regulation by a class of noncoding RNAs. MicroRNAs (miRNAs) are functional RNAs with 18–25 nt in length that contribute to a class of cellular functions by negatively controlling targeted gene expression via base-pairing to 3′ untranslated region (3′ UTR). A single miRNA regulates the expression of multiple genes, and the functions of miRNAs therefore need to be orchestrated for cellular homeostasis (Ventura and Jacks, 2009). In the context of cancer pathology, many studies have provided evidences that miRNAs can act as either oncogenes or tumor suppressors. Although the relationship between miRNA deregulation and oncogenes has been clarified in several cancer cells, there has been no integrated analysis of gene expression in ATL. Since miRNAs have important functions in living cells, miRNA expression needs to be tightly regulated. Our knowledge about the regulatory mechanisms of miRNA expression is very inadequate because research effort has focused mainly on the role of miRNAs, which remains one of the most intriguing questions. miRNA regulation involves multiple steps. miRNA maturation has been identified as an important step, and its deregulation leads to progression and development of cancer (Davis et al., 2008; Trabucchi et al., 2009). Genetic deletion in cancer cells has also been reported to account for specific miRNA defect (Varambally et al., 2008). In addition, miRNA expression seems to be epigenetically programmed. DNA methylation and histone modification are strong candidates for miRNA regulation and their abnormalities, therefore, have causal roles in cancer initiation, development, and progression. In particular, Polycomb group proteins have central functions in cellular development and regeneration by controlling histone methylation, especially at histone H3 Lys27 (H3K27), which induces chromatin compaction (Simon and Kingston, 2009). Recent studies have revealed that the amount of Polycomb family is closely associated with cancer phenotypes and malignancy in breast cancer, prostate cancer, and other neoplasms (Sparmann and van Lohuizen, 2006). However, the substantial status of Polycomb family and their epigenetic impact in ATL cells have not been documented. Furthermore, the general roles of Polycomb proteins in miRNA regulation are mostly unknown. As described above, since miRNAs are multifunctional molecules in gene regulation, it is of pivotal importance to clarify the miRNAs functions and their regulatory circuit in order to formulate therapeutic strategies.

In the present study, we first performed global miRNA and mRNA profilings of the ATL cells derived from patients to precisely define the significance of miRNA expressions and functions.

RESULTS

miRNA Expression Signature in Primary ATL Cells

To characterize the miRNA expression signature in the primary ATL cells, we first performed an miRNA expression microarray analysis. For results with physiological significance, we used total RNA prepared from clinical ATL samples (n = 40, Table S1 available online) and control CD4+ T cells from healthy donors (n = 22) aged 50–70 years. A strict threshold ($p < 1 \times 10^{-5}$) and two-dimensional hierarchical clustering analysis revealed 61 miRNAs that showed significantly altered levels of expression in ATL cells compared with those of control CD4+ T cells (Figure 1A). It is noteworthy that 59 miRNAs out of 61 (96.7%) showed decreased expression in the primary ATL cells. Among them, we identified miR-31 as one of the most profoundly repressed miRNAs in all ATL individuals (fold change, 0.00403; Figure 1B). miR-31 was recently reported as a tumor suppressor and/or metastasis-associated miRNA in metastatic breast cancer. However, the biological functions of miR-31 in lymphocytes have not been studied. We therefore focused on the biological significance and regulatory mechanisms of miR-31 expression in T cells as well as in solid cancers.

miR-31 Negatively Regulates NF-κB Signaling via NIK Expression

To study the functional significance of miR-31 loss, we attempted to identify the target genes of miR-31 using four computational algorithms. We also performed gene expression microarray analysis of the primary ATL cells (n = 52, Table S1) and normal CD4+ T cells (n = 21) in order to detect aberrations in gene expression. Selected putative target genes are known to be involved in cell-cycle regulation and T cell development (Table S2). To experimentally identify the target genes, we performed reporter-based screens as described below. Luciferase-3′ UTR reporter assays demonstrated a remarkable negative effect against upstream gene expression by the *MAP3K14* 3′ UTR sequence (Figure S1B), which is consistent with an initial cloning report (Malinin et al., 1997). MAP3K14, also known as NIK, has a central role in noncanonical NF-κB signaling by phosphorylation of IKKα. A previous report (Saitoh et al., 2008) and the present results (Table S2) show that NIK is overexpressed in ATL cells, leading to constitutive NF-κB activation. As shown in Figure 2A, treatment with a miR-31 inhibitor increased *NIK* 3′ UTR reporter activity, suggesting the involvement of endogenous miR-31 in NIK downregulation. A computational search predicted one site each of miR-31 and miR-31 antisense (miR-31*) binding sites in the *NIK* 3′ UTR (Figure 2B). To identify the regulatory sequence in 3′ UTR of *NIK*, we established additional two reporters with mutated sequence in each potential seed region (Figure 2C; Figure S1C). Mutant 1, which contains mutated sequence in the miR-31 seed region, partially canceled the negative effect of endogenous miR-31 (Figure S1D) and prevented the effect of Anti-miR-31 treatment (Figure 2D). On the contrary, our results suggest that miR-31* does not participate in NIK regulation. miR-31-mediated reporter regulation was also observed in T cell lines (Figure S1E). To confirm the results, we repeated the experiment to examine whether miR-31 could inhibit NIK expression through seed sequence. We made expression plasmid vectors carrying NIK, NIK-3′

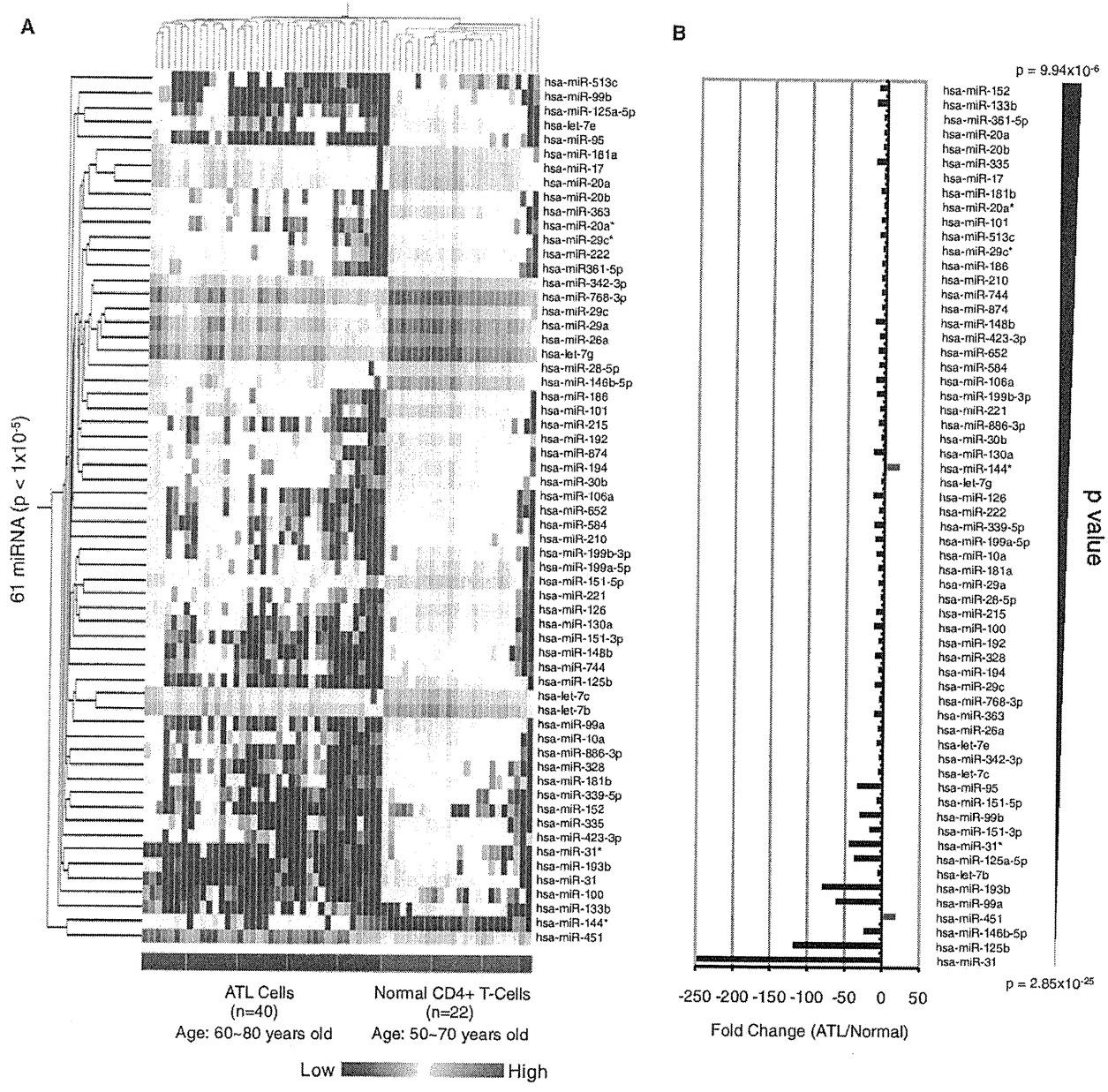

Figure 1. Global Profiling of Cellular miRNA on Primary ATL Cells

(A) Two-dimensional hierarchical clustering analysis and Pearson correlation as similarity measure on the miRNAs expressed at significantly different levels between the ATL (n = 40) and the control (n = 22) groups. Sixty-one miRNAs were identified ($p < 1 \times 10^{-5}$) and by filtering on more than 5-fold changes. A vertical branch shows the expression pattern of the selected miRNAs in each individual.

(B) Fold changes in the 61 miRNAs between ATL and Normal ($p < 10^{-5}$, fold change >5-fold). Selected miRNAs are arranged according to p values. See also Table S1.

UTRWT, or NIK-3′ UTRMu1 and tested their expressions in 293T cells. Results demonstrated that expression of NIK-3′ UTRWT was inhibited by simultaneous introduction of miR-31 (Figure 2E). miR-31 inhibition inversely rescued the NIK level, revealing that the cellular miR-31 level negatively affected that of the NIK protein through its 3′ UTR sequence. These lines of evidence collectively demonstrated that miR-31 recognizes and regulates *NIK* mRNA through specific binding to its 3′ UTR.

Transient introduction of the miR-31 precursor in TL-Om1 cells, which were established from an ATL patient, resulted in downregulation of NIK at the mRNA and protein levels, associated with downregulation of the phospho-IKKα/β level and NF-κB activity (Figures S1F and S1G). In contrast, miR-31 inhibition resulted in accumulation of NIK mRNA and protein in HeLa cells (Figure 2F). Manipulation of the miR-31 level clearly indicated that the miR-31 level negatively correlates with cellular

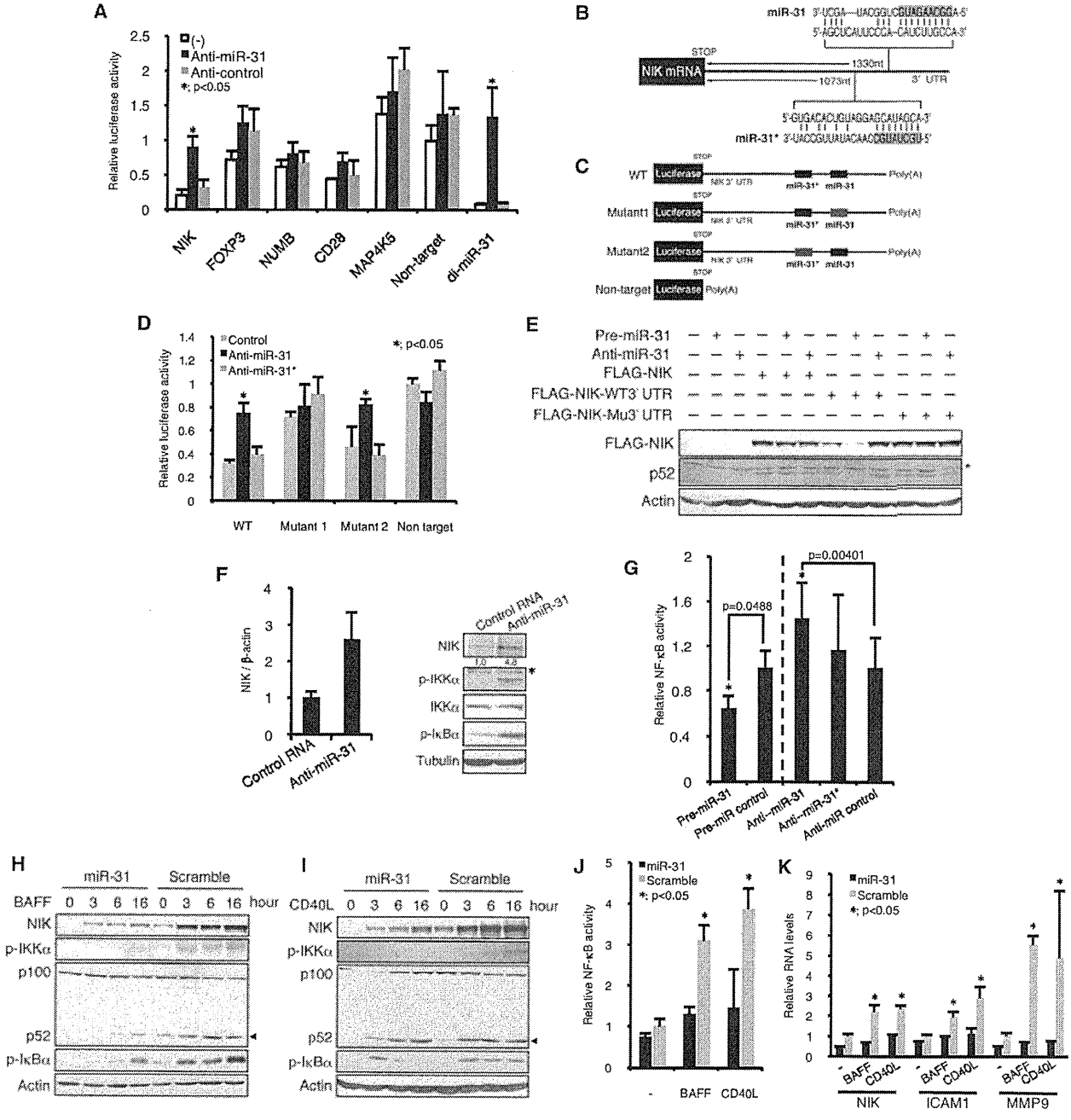

Figure 2. miR-31 Is a Negative Regulator of NF-κB Pathway by Inhibiting NIK Expression

(A) Reporter-based miR-31's target gene screening. A series of 3′ UTR-luciferase reporters was transfected in HeLa cells together with or without miR-31 specific inhibitory RNA (Anti-miR-31) or control RNA (Anti-control). Relative values of Dual-luciferase assay are presented. "Non-target" represents reporter without any 3′ UTR. "di-miR-31" reporter contains two perfect match sequences. The data are presented as mean ± SD of three independent experiments.

(B) Schematic of miR-31 target sites in the *NIK* 3′ UTR.

(C) Mutation-induced reporters. Red box stands for mutated target region (see Figure S1C).

(D) miR-31 negatively regulates *NIK* 3′ UTR analyzed by reporter assay (n = 4, mean ± SD). Luciferase activities of reporter series were tested in a presence or absence of miR-31 inhibitor.

(E) FLAG-tagged NIK protein is negatively regulated through its 3′ UTR and miR-31 binding. Plasmid vectors and miR-31 precursor or miR-31 inhibitor are cotransfected in 293T cells. Western blots showed levels of NIK and endogenous p52. Asterisk indicates nonspecific bands.

(F) NIK mRNA (left) and protein (right) levels in HeLa cells measured by quantitative RT-PCR (n = 3, mean ± SD) and western blotting, respectively. Treatment of miR-31 inhibitor resulted in NIK accumulation. Result of densitometry is shown in the bottom panel. Asterisk indicates nonspecific bands.

(G) Cellular NF-κB activity in HeLa cells (n = 5, mean ± SD) in a presence or absence of miR-31 precursor or inhibitor.

NF-κB activity (Figure 2G). Furthermore, enforced miR-31 expression in B cells attenuated both BAFF and CD40L-mediated NIK accumulation and the subsequent NF-κB signaling (Figures 2H–2K). Consistent with previous reports (Ramakrishnan et al., 2004; Zarnegar et al., 2008b), we also found decreased levels of IκBα phosphorylation. On the other hand, TNF-α-triggered canonical NF-κB activation was not affected by miR-31 in Jurkat cells (Figures S1H–S1K). These results collectively show that miR-31 inhibits the basal and receptor-initiated activities of noncanonical NF-κB pathway. With genetic evidence and an experimental approach, we further demonstrated that the function of miR-31 is well conserved among several classes of species (Figures S1L–S1O). Taking together all these results, miR-31, which is almost completely absent in primary ATL cells, appears to play a critical role in negative regulation of the NF-κB pathway by manipulating the expression of NIK.

miR-31 Suppresses ATL Cell Growth and Promotes Apoptosis by Inhibiting NF-κB

Although it was documented that abnormal NIK accumulation in ATL cells acts as a constitutive activator of the NF-κB pathway, the mechanism underlying overproduction of NIK remains to be elucidated. The results described in the previous section indicated that the amount of miR-31 is linked to the level of NIK, and we therefore speculated that downregulation of miR-31 expression is at least partially responsible for the constitutive activation of NF-κB in ATL cells. Quantitative RT-PCR revealed that *NIK* mRNA levels were negatively correlated with miR-31 levels in primary ATL cell samples (Figure 3A). To investigate the functional roles of NIK and miR-31, we established TL-Om1 cells stably expressing the miR-31 or NIK specific shRNA (shNIK) by retroviral vectors. RT-PCR and western blots showed that expression of miR-31 or shNIK reduced NIK at mRNA and protein levels as well as the levels of phospho-IKKα/β, p52, and IκBα (Figures 3B and 3C). Decreased levels of nuclear RelA and RelB are considered to represent repressed activities of the canonical and noncanonical NF-κB pathways, respectively (Figure 3D). EMSA and NF-κB reporter assays also revealed the repressive function of miR-31 and shNIK on the NF-κB activity (Figures 3E and 3F; Figures S2A, S2B, S5B, and S5C). Re-expression of NIK led to NF-κB activation that was inhibited by miR-31, suggesting a reciprocal relationship between the level of miR-31 and that of NIK.

We and others previously showed that constitutive NF-κB activation is a strong driver of ATL proliferation and prosurvival properties. Here, we examined the effects of miR-31 loss on ATL cell growth. We found that TL-Om1 cells expressing miR-31 or shNIK showed a significant attenuation of cell proliferation compared with control cells. In addition, serum starvation experiments showed greater sensitivity to induced cell death in NIK-repressed cells (Figure 3G). miR-31 expression showed the same phenotypic results in other ATL-derived cell lines (Figures S2C, S2D, and S5E). Jurkat cells do not have significant basal activity of NF-κB, and showed no significant difference in cell growth with or without induced expression of miR-31 (Figure S2E).

Next, we hypothesized that miR-31-mediated NF-κB modulation may affect cellular apoptosis, because numerous studies have demonstrated that NF-κB activation is a strong antiapoptotic factor in ATL and other cancer cells. We found that repression of NIK by miR-31 or shNIK resulted in downregulation of a subset of genes involved in resistance to apoptosis such as BCL-XL, XIAP, and FLIP (Figure 3H), suggesting that miR-31 has a role in proapoptosis through inhibition of NF-κB activity. To assess the biological function of miR-31 in apoptosis signals, we utilized a lentivirus gene transfer system for cell lines and freshly isolated tumor cells. The lentivirus vector is competent to infect nondividing cells and the infected cells can be monitored by the fluorescence of Venus. We found that lentivirus-mediated miR-31 expression promoted basal and Fas-directed apoptosis in TL-Om1 cells (Figure 3I). Venus-negative population showed no significant changes, demonstrating the specificity of miR-31 activity. To confirm the relationship among miR-31, NIK, and NF-κB signaling, we also prepared another retroviral vector encoding NIK without its 3′ UTR sequence. As results, re-expression of NIK reversed the miR-31-mediated apoptosis. In addition, miR-31 expression led to caspase 3 activation (Figure 3J). Collectively, these findings indicate that miR-31 mediates apoptosis through repression of NIK in ATL cell lines.

Tumor cells from ATL patients primarily represent the malignant characteristics. In fact, miR-31 loss is found from patient samples (Figures 1 and 3A). To demonstrate the responsibility of miR-31 for tumor cell survival, we tested whether lentivirus-mediated miR-31 expression has a killing effect against tumor cells. After establishment of lentivirus infection, the apoptotic cells were determined by flow cytometry. The results revealed that expression of miR-31 facilitated tumor cell death. Since NIK repression by shRNA lentivirus also showed a strong killing effect, NIK and NF-κB activity are suggested as crucial players for survival in ATL tumor cells (Figure 3K). Strong toxicities were not observed in normal resting lymphocytes that express low levels of NIK. Taken together, these lines of experimental evidence, including data from cell lines and primary ATL cells, definitively support two notions that (1) miR-31 acts as a tumor suppressor in T cells, and (2) NIK-regulated NF-κB has pivotal importance in cancer cell survival.

Loss of miR-31 Occurs in T Cells with Genetic and Epigenetic Abnormalities

The results described above together with previous publications indicate that regulation of miR-31 expression has profound impacts on multiple functions in human tumors as well as in normal cells. However, little is known about the regulatory mechanism of miR-31 expression. The human gene that encodes miR-31, *hsa-miR-31*, is located at 9p21.3, which is

(H–K) miR-31 attenuates signal-dependent NF-κB activation in B cells. (H and I) BJAB cells expressing miR-31 or control RNA were treated with BAFF (0.2 μg/ml) or CD40L (0.5 μg/ml) for indicated time periods. The protein levels of NIK, phospho-IKKα/β, p100/p52 (arrowheads indicate active p52), and phospho-IκBα were shown. Actin was detected as control. (J) NF-κB activity (n = 5, mean ± SD) evaluated by NF-κB-luciferase reporter assay at 24 hr after cytokine treatments. (K) NF-κB-dependent gene expressions were inhibited by miR-31 (n = 3, mean ± SD). See also Table S2 and Figure S1.

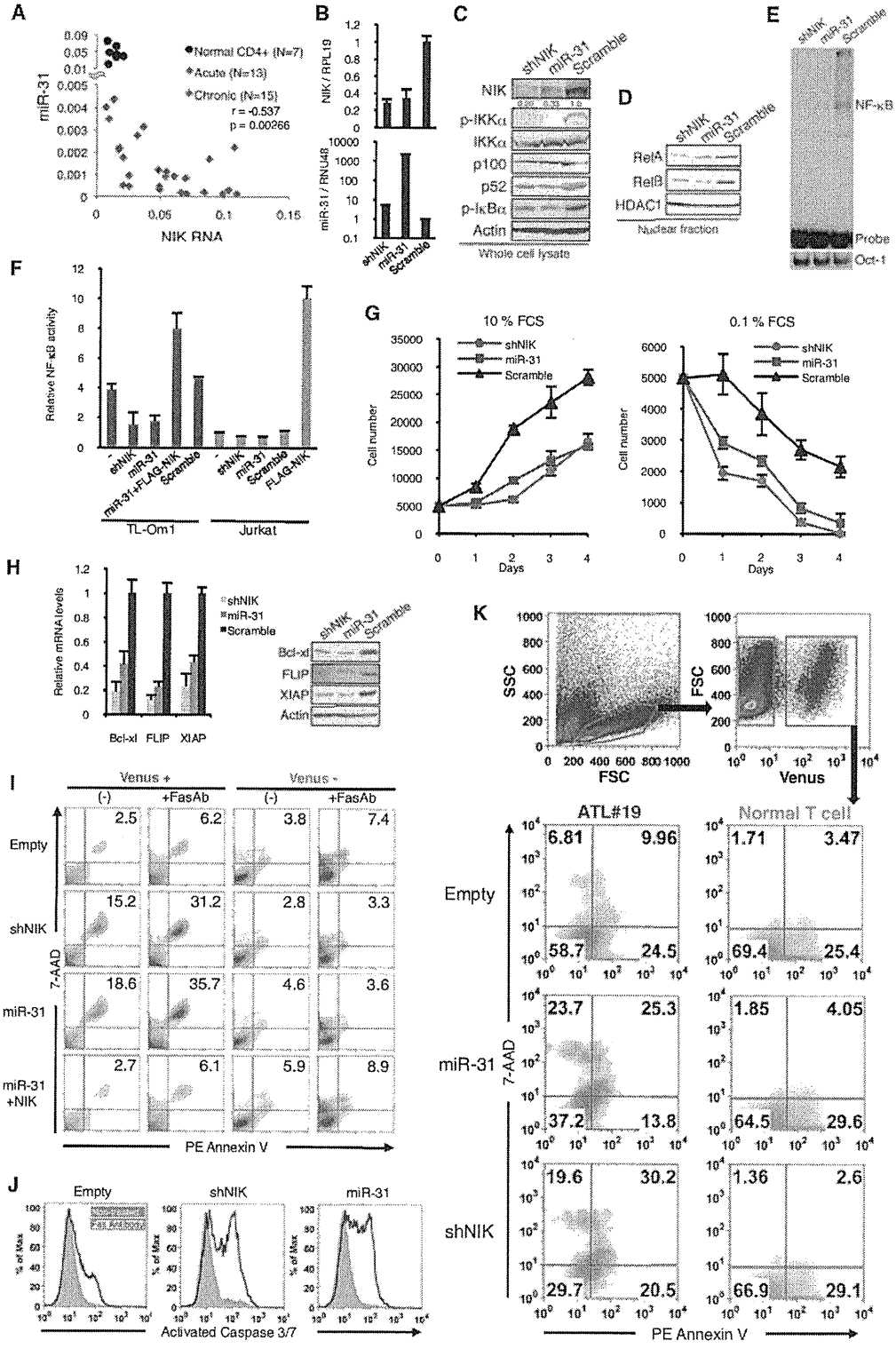

Figure 3. Loss of miR-31 Is Responsible for Constitutive NF-κB Activation, Abnormal Cell Growth, and Resistance to Apoptotic Cell Death in ATL Cells

(A) Expression levels of miR-31 and *NIK* in individual ATL patients and normal controls using data set obtained by quantitative RT-PCR. Pearson's correlation coefficient within ATL samples was described in the graph.